University of North Dakota
UND Scholarly Commons

Earth System Science and Policy Faculty Publications

Department of Earth System Science and Policy

6-2018

Diel variations of the attenuation, backscattering and absorption coefficients of four phytoplankton species and comparison with spherical, coated spherical and hexahedral particle optical models

Carina Poulin

Xiaodong Zhang
University of North Dakota, xiaodong.zhang2@UND.edu

Ping Yang

Yannick Huot

Follow this and additional works at: https://commons.und.edu/essp-fac

Recommended Citation

Poulin, Carina; Zhang, Xiaodong; Yang, Ping; and Huot, Yannick, "Diel variations of the attenuation, backscattering and absorption coefficients of four phytoplankton species and comparison with spherical, coated spherical and hexahedral particle optical models" (2018). *Earth System Science and Policy Faculty Publications*. 6.
https://commons.und.edu/essp-fac/6

This Article is brought to you for free and open access by the Department of Earth System Science and Policy at UND Scholarly Commons. It has been accepted for inclusion in Earth System Science and Policy Faculty Publications by an authorized administrator of UND Scholarly Commons. For more information, please contact zeineb.yousif@library.und.edu.

Journal of Quantitative Spectroscopy & Radiative Transfer 217 (2018) 288–304

Contents lists available at ScienceDirect

Journal of Quantitative Spectroscopy & Radiative Transfer

journal homepage: www.elsevier.com/locate/jqsrt

Diel variations of the attenuation, backscattering and absorption coefficients of four phytoplankton species and comparison with spherical, coated spherical and hexahedral particle optical models☆

Carina Poulin[a,*], Xiaodong Zhang[b], Ping Yang[c], Yannick Huot[a]

[a] Université de Sherbrooke, 2500, boulevard de l'Université, Sherbrooke, Québec J1K 2R1, Canada
[b] University of North Dakota, Clifford Hall Room 326, 4149 University Ave Stop 9011, Grand Forks, North Dakota 58202-9011, USA
[c] Department of Atmospheric Sciences, Texas A&M University, TAMU-3150, College Station, Texas 77843, USA

ARTICLE INFO

Article history:
Received 10 April 2018
Revised 24 May 2018
Accepted 29 May 2018
Available online 15 June 2018

Keywords:
Phytoplankton
Optical properties
Backscattering
Attenuation
Models
Spherical
Coated
Hexahedral
Diel variations
Diurnal

ABSTRACT

Diel variations of inherent optical properties (absorption coefficient, attenuation coefficient and volume scattering function at 124°) of four species of phytoplankton were measured in the laboratory and were simulated using a homogeneous spherical model, a coated spherical model and a homogeneous hexahedral model. The required inputs to run each optical model were acquired from the measurements; the real and imaginary parts of the refractive index were determined from the intracellular carbon and absorption coefficient, and particle size distributions from the Coulter counter. We conducted a sensitivity analysis on the inherent optical properties in response to changes in the slope of Junge distributions that were used to represent non-phytoplankton particles of radii less than 1.12 µm (the minimum size of the Coulter counter), realistic maximum and minimum values of the refractive indices used for the shell and core, shell thickness, cell radius and the number of cells. We found that the shell's refractive index is the most important factor influencing the backscattering ratio. We found that the coated spherical model reproduced the observed optical properties best for all species possessing a shell. The hexahedral and homogenous spherical models give relatively good results for the absorption and attenuation coefficients; but underestimated the volume scattering function at 124°. Correlations between the measured backscattering cross sections and carbon are significant only for *E. huxleyi* and *D. tertiolecta*. In situ measurements will be necessary to determine if our models can reproduce the diel variations of backscattering that are observed in the ocean.

© 2018 The Authors. Published by Elsevier Ltd.
This is an open access article under the CC BY-NC-ND license.
(http://creativecommons.org/licenses/by-nc-nd/4.0/)

1. Introduction

Phytoplankton are responsible for close to half of the world's primary production [1]. They are ubiquitous in all surface waters of the world, making remote sensing the only tool amenable to their monitoring at the global scale. This is generally done by measuring the reflectance of the water in the visible wavelengths. The reflectance, in turn, is determined by the inherent optical properties (IOPs) of the water and the observation conditions and geometry [2–4]. These inherent optical properties form the link between the constituents of the water, including phytoplankton, and the reflectance. Phytoplankton IOPs show diel variations in nature [5–13]. The ocean diel variations of the IOPs are in part influenced by cycles of biomass due to daily photosynthesis leading to larger cells [14–16], cell division [17,18] and nightly grazing and respiration (e.g., [6]). They have been used to compute phytoplankton or community production (e.g., [5,14]) non-intrusively. This study focuses on the diel changes of both phytoplankton biomass and their physiology that influence IOPs.

The main IOPs of ocean water are the absorption coefficient (a, m^{-1}) and the volume scattering function (VSF or β, m^{-1} sr^{-1}) [19]. They are additive, meaning that, for example, the total absorption coefficient (a, m^{-1}) is the sum of the absorption coefficient of water, dissolved matter and particles (a_p, m^{-1}). The volume scattering function represents the angular scattering amplitude and is often integrated from 0° to 90° to obtain the forward scattering coefficient, from 90° to 180° to obtain the backscattering coefficient

☆ Competing interests statement: none

* Corresponding author.
E-mail addresses: carina.poulin@usherbrooke.ca (C. Poulin), zhang@aero.und.edu (X. Zhang), pyang@tamu.edu (P. Yang), yannick.huot@usherbrooke.ca (Y. Huot).

https://doi.org/10.1016/j.jqsrt.2018.05.035
0022-4073/© 2018 The Authors. Published by Elsevier Ltd. This is an open access article under the CC BY-NC-ND license. (http://creativecommons.org/licenses/by-nc-nd/4.0/)

(b_b, m^{-1}) and from 0° to 180° to obtain the total scattering coefficient (b, m^{-1}). The ratio b_b/b is referred to as the backscattering ratio. The β measured near 120° can also be used as a proxy for b_b [20–23]. The sum of a and b is the attenuation coefficient (c, m^{-1}). IOPs are independent from lighting conditions and can be measured in the laboratory or in situ. They can be used to obtain biological information about the constituents of water such as pigmentation (e.g., [24]), cell size (e.g., [21]) and carbon content (e.g., [8,10,25–27]).

1.1. Particle models for IOPs

Particle models for IOPs are used to simulate the optical effect of water constituents. The simplest model assumes that particles are homogeneous spheres. It has been frequently used to simulate phytoplankton optical properties based on the Lorenz–Mie scattering theory (e.g., [28–33]). It has, however, been found to underestimate the backscattering coefficient [34–39].

The underestimation of the backscattering coefficient by particles represented by spheres could, at least in part, be responsible for what has been referred to as the "backscattering enigma", the observation that the measurements of backscattering are significantly higher than predictions from the Lorenz–Mie theory [40,41]. This observation has led to the speculation that small detrital particles, which are known to be abundant in the ocean should be responsible for most of the measured backscattering [30,31,42]. Particles in the size range of phytoplankton could, however, be a more significant source of backscattering than originally thought [34,38,39,41,43–47]. Relationships between the particulate backscattering coefficient (b_{bp}, m^{-1}) and chlorophyll concentration have also been observed in clear ocean waters (e.g., [48]), which could indicate a direct influence of phytoplankton on b_{bp} or a strong covariation of small particles with phytoplankton abundance.

Beyond homogeneous spheres, more complex particle models have also been used to represent phytoplankton. They vary in their representation of particle shapes and internal structure.

1.1.1. Particle shape and more complex models

Phytoplankton shapes are diverse [49,50] and directly influence their optical properties [39,43]. To calculate scattering from non-spherical models, computational techniques such as the *T*-matrix method [51] are used. These models have shown that backscattering is sensitive to shape [37,52]. The discrete dipole approximation has also been used to model disk-like shapes to represent coccolithophores [53] and coccoliths [54,55]. Bi and Yang [56] used the invariant imbedding T-matrix method to simulate the optical properties of coccolithophores and coccoliths with various degrees of calcification. The Schiff approximation has been used to represent phytoplankton of complex shapes [57]. An hexahedral particles model [58] has also shown promise for aerosol particles and has been applied to aquatic particles [59,60] and the inversion of volume scattering functions of oceanic and coastal particles [61,62]. For particle aggregates, the Generalized Multiparticle Mie-solution (GMM) model calculates scattering for aggregates based on the Lorenz–Mie theory [63].

The models with complex shapes mentioned above have shown reasonably good agreement with measurements of IOPs, including backscattering. However, they generally require lengthy calculations. Quirantes and Bernard [64] showed that a relatively simple layered spherical model representing the internal structure of phytoplankton produced results that were very similar to those from a model of randomly oriented coated spheroids for both b and b_b.

1.1.2. Representing cell structure in models

Adding a coating to the homogenous sphere models to represent cell membranes, frustules in the case of diatoms, or coccoliths for coccolithophores increases the backscattering ratio [34,37,44,65,66]. Other two layer models also treat chloroplasts as an outer layer [45,64,67] or as the core [35] or the core as a gas vacuole [68]. Three-layer models have also been studied, representing cytoplasm, chloroplasts and cell wall [34,35,67] or nucleus, cytoplasm and cell wall [69].

Multilayered models show that backscattering tends to increase significantly when adding cellular structure [35] while absorption and attenuation remain similar to homogeneous models. As mentioned above, the latter two are generally well modeled by homogeneous spherical models but backscattering is underestimated [35,37,70,71].

1.1.3. Refractive indices in models

The dimensionless complex refractive index (m) of phytoplankton is represented as,

$$m(\lambda) = n(\lambda) + i \cdot n'(\lambda), \quad (1)$$

where λ (nm) is the wavelength, n is the real part of the refractive index, representing the phase velocity of the wave and n' is the imaginary part, representing absorption. Herein, we always provide values for the refractive indices relative to water ($n = 1.334$).

Refractive indices of phytoplankton and other oceanic particles vary depending on internal contents and composition [72]. The real part of the refractive index is generally linked to the internal carbon concentration of planktonic organisms [73–75] and the imaginary part to pigmentation. The real part of the refractive index of phytoplankton cells can be measured in the laboratory by immersion of particles in liquids of different refractive indices until the edges of the particles disappear [76]. The known refractive index of the liquid will be associated to the particle. However, the method does not work well for inhomogeneous particles [72,76] and is laborious.

The real part of the refractive index can also be derived through an iterative search method based on the Lorenz–Mie scattering theory or its anomalous diffraction approximation (e.g., [29,32,70,71,73–75,77,78]). Because these methods use spherical models to determine refractive index of particles, they are not ideal for a study (such as ours) whose objective is to assess the applicability of particle models to simulate scattering by phytoplankton. They are, however, more accessible than the direct measurements and provide an acceptable approximation most of the time.

1.1.4. Cell size distributions in models

Distributions of biological populations typically follow a log-normal distribution [79]. In the ocean, numerous populations of phytoplankton and other particles coexist, each with their own log-normal distribution of various sizes. The sum of the concentration all particles roughly follows a power-law function (e.g., [80]), and Junge distributions of particle size distribution with exponent between 2.5 and 5 are often used to model bulk particle size distributions in the ocean [81]. Sometimes the Junge distribution is broken down with different power law exponents for particles of diameters smaller and bigger than 6 µm [82,83]. Such simplified distributions are often used in modeling IOPs instead of measurements of particle size distributions. This, however, is inevitably a source of differences between the models and measurements because most natural distributions always depart from these idealized representations.

1.2. Using diel variations in cultures to study optical models

Cultures of phytoplankton allow the study of phytoplankton in controlled conditions, minimizing the presence of other mineral or

detrital particles (especially in exponential phase and when proper care is taken). Consequently, they can help to identify the factors influencing the IOPs which follow diel variations in laboratory experiments [74,75,84,85] as well as in nature [5–15].

In a previous study using the same cultures as presented herein, Poulin et al. [86] observed diel variations of b_{bp} suggesting that phytoplankton could at least partly drive the diel (or diurnal, i.e. during daylight) variations of b_{bp} that are observed in nature [16]. Those b_{bp} variations can also be used to study the factors that influence the applicability of different particle models to phytoplankton IOPs.

2. Objective

We aim to evaluate the applicability of various particle models in reproducing the diel changes of the optical properties of phytoplankton especially the backscattering coefficient. The particle models to be tested include homogeneous spheres, coated spheres and homogeneous asymmetric hexahedra. The homogeneous sphere and asymmetric hexahedra represent almost diametric extremes in terms of particle shapes: symmetry vs. non-symmetry and smooth curve vs sharp edges. The use of coated sphere will test the homogeneity vs heterogeneity. The refractive indices and particle size distributions that are needed to calculate the bulk optical properties of phytoplankton species are derived from the ancillary measurements.

3. Materials and methods

3.1. Experiments

The experiments were carried out to observe the diel variations of the optical properties of four species of phytoplankton. The details of the experiment were described in Poulin et al. [86] and here we provide a brief summary. The cultures were semi-continuous and maintained in exponential phase by diluting once a day with sterile culture medium for at least 10 generations to reach steady-state. Growth irradiance was provided by fluorescent tubes and computer-controlled to vary in intensity following a sinusoidal curve with a maximum of 400 µmol photons m^2 s^{-1} outside the vessels and a 14 h day/10 h night cycle. Multiple samplings were carried out during a day starting one hour before sunrise and ending one hour after sunset.

We measured chlorophyll a concentration (Chl) by fluorometry using the non-acidification method [87,88]. Cell counts and diameters were measured using a Multisizer 4 Coulter Counter (Beckman Coulter, USA) equipped with a 100 µm aperture tube and calibrated with 5 µm polystyrene beads (Fig. 1a). Cultures were diluted approximately 100 times (depending on the species) with a twice-filtered 35% NaCl Milli-Q solution before counting. Samples for carbon were filtered on pre-cremated filters and decarbonated and dried before their analysis in a Fisons - EA-1108 CHNS-O Element Analyzer (Thermo Scientific, USA).

For optical measurements, a setup made up of a 7 L black bucket, an ac-s (Wet Labs, USA) connected by silicone tubing and a peristaltic pump was used while the ECO BB9 backscattering meter (Wet Labs, USA, wavelengths: 407, 439, 485, 507, 527, 594, 651, 715, 878 nm) was placed over the bucket, measuring heads in the water, facing down. We made sure that the sides of the bucket did not influence the ECO BB9 by checking stability of measurements while moving the instrument around (with filtered water and in the presence of algae). A recirculation loop with a 0.2 µm capsule filter was used for filtration between the bi-hourly sampling timepoints.

We poured a volume of the culture sample varying between 50 mL and 200 mL (depending on the scattering of the cultures during previous tests) in the 7 L bucket and lightly but thoroughly mixed the contents and removed any bubbles on the heads of the ECO BB9 by wiping carefully with a squeegee before measuring simultaneously with the ac-s and the ECO BB9. We obtained the total volume scattering function at 124° ($\beta(124)$, m^{-1}) from the ECO BB9 counts by interpolating between the pre experiment and post-experiment factory calibration values. We subtracted Zhang et al. [89] volume scattering function of pure water to obtain the volume scattering function of particles ($\beta_p(124)$, m^{-1}). The particulate backscattering coefficient (b_{bp}, m^{-1}) was calculated as

$$b_{bp} = 2\pi\ \chi\ \beta_p(124), \tag{2}$$

where we used 1.076 [90] for the proportionality constant χ.

While the bucket content was filtered between each bi-hourly sampling to return to blank values, this was not done between each sample (two cultures in three replicates were measured at each time point). Therefore, for each sample, the particulate absorption coefficient ($a_{\boldsymbol{p}}$, m^{-1}), the attenuation coefficient ($c_{\boldsymbol{p}}$, m^{-1}) and b_{bp} of the preceding sample was subtracted to obtain the particulate coefficients of the measured sample.

3.2. Theoretical optical properties

We simulated the diel variations of the internal carbon concentration optically by changing the real part of the refractive index of the particle cores. For each species, we used the maximum and minimum refractive indices reported in Aas [72], averaged them and linearly regressed them against the maximum, minimum and average intracellular carbon concentration (Mass/Volume, µg/µm^3) measured in our experiments. Using this relationship, we computed the refractive index for each time point from the measured intracellular carbon concentration. We used the mean of the 3 cultures at every time point for the simulations (Fig. 1b).

Following Morel and Bricaud [28] and Stramski and Reynolds [74], the imaginary part of the refractive index (n') was calculated using Eqs. (3)–(6) for every culture at each time point for the wavelengths measured with the ECO BB9 (Fig. 1c). We used the experimental data to obtain the intracellular chlorophyll concentration (Chl_i, mg m^{-3}), the chlorophyll-specific absorption coefficient (a_p^{Chl}, m^2 mg^{-1}) and the cell diameter (D, m) using Eq. (3):

$$n' = \rho'\,(4x)^{-1} \tag{3}$$

$$\rho' = D\,a_{cm}\,(\lambda), \tag{4}$$

$$x = \pi\,D\,n_w\,\lambda^{-1} \tag{5}$$

$$a_{cm}\,(\lambda) = a_p{}^{Chl}\,Chl_i \tag{6}$$

where ρ' is the optical thickness parameter, x is the size parameter, n_w is the refractive index of water (1.334), and a_{cm} is the absorption coefficient of the cellular material. The refractive index (m) was thus calculated with Eq. (1). The n of the shell (n_{shell}) for the diatoms was set to 1.1 (representing opal; [72]). Even though *Dunaliella* cells do not possess a shell per se, to evaluate the performance of the coated sphere model across all the species, we assigned a refractive index of 1.08 corresponding to the shell of *Chlorella*, another genus of green algae, for the n_{shell} of *D. tertiolecta*.

We did not include an imaginary part to the refractive index of the shells, since pigments are found within the cells. The thickness of the shells (r_{shell}, µm) was fixed at 0.1 µm for the diatoms [91] and 0.1 µm for *E. huxleyi*, which is on the lower end of observed values in cultures [92]. For the hexahedral model, we averaged the real part of the refractive index of the core with the n_{shell} and used it for the whole cell.

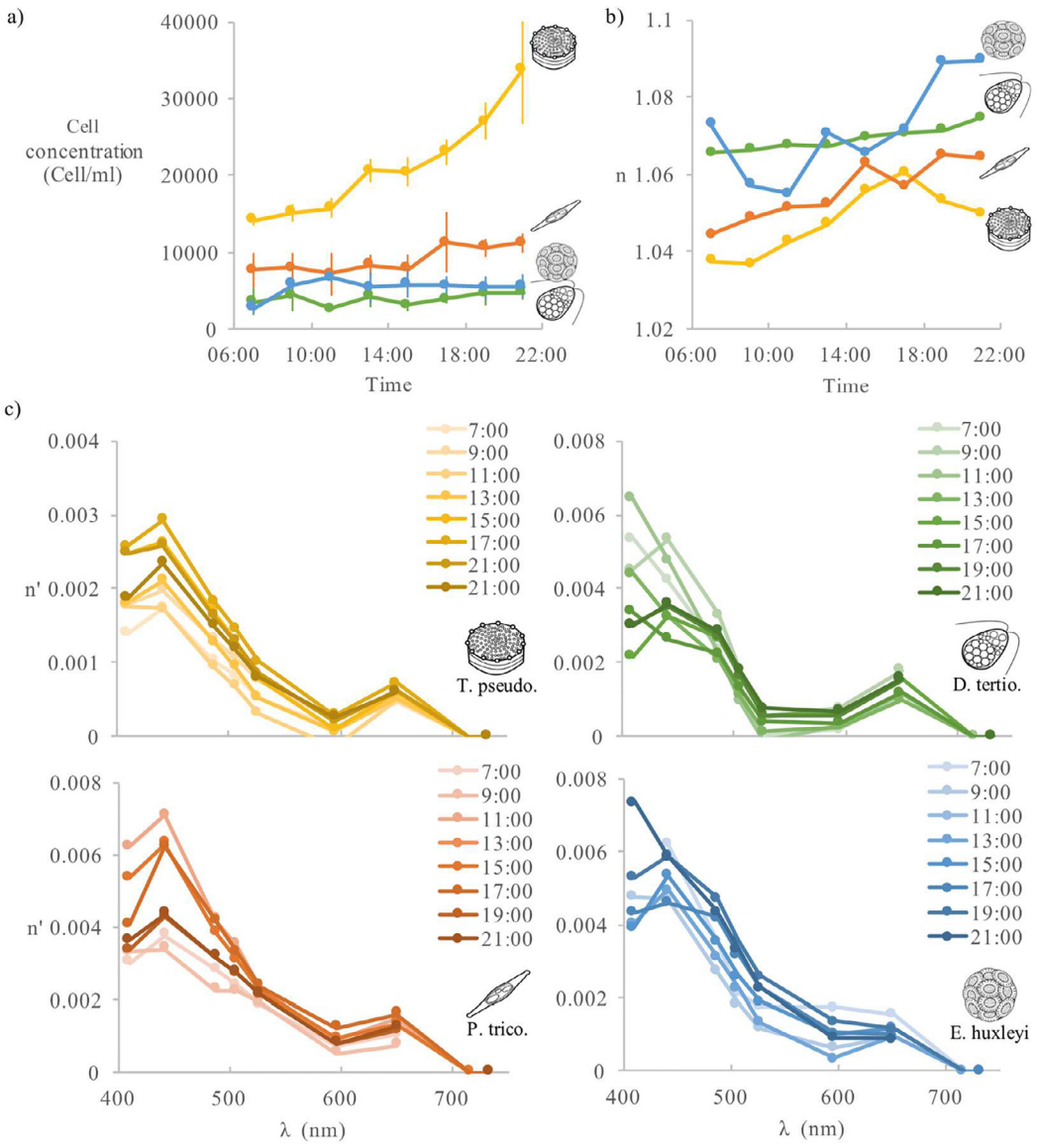

Fig. 1. Diel variations of (a) the cell concentration in the IOP measurement container. (b) the real and (c) the imaginary part of the refractive indices estimated from the measurements of intracellular carbon and chlorophyll concentrations.

3.2.1. Simulating the IOPs

The use of the experimental and theoretical data to simulate the IOPs is described in Fig. 2. For the spherical particle model simulations, we used a Matlab code developed by Zhang [93], which allows the numerical computation of scattering phase function of spherical particles with a coating based on the Lorenz–Mie scattering theory. The hexahedral particle model simulations were carried out with a function developed by Zhang et al. [23] based on precomputed results for asymmetrical hexahedral particles from the model developed by Bi et al. [94].

We used the entire cell size distributions obtained from the Multisizer 4 Coulter Counter (Beckman Coulter, USA) (see Poulin et al. [86]) in volume equivalent spherical diameters to calculate the IOPs from the optical efficiencies obtained by the models. It is worth noting that the species that were not spherical (*T. pseudonana* and *P. tricornutum*) had slight shoulders in their cell size distributions due to changes in orientation. When we added a coating to the model, we kept the measured total radius of the cells and subtracted the shell's thickness to obtain core radius in the calculations.

For comparison between simulated and measured IOPs with the ac-s, we adjusted the modelled b_p values to account for the acceptance angle of the ac-s by removing the integrated β_p values between 0° to 0.9° from simulated scattering coefficients [61].

We did not include the spectral dependence of the real part of the refractive index in the models. This is not likely to have a significant impact on the results [32].

3.2.2. Sensitivity analysis

To examine the impact of changes of different model parameters over a realistic or expected range, we carried out a sensitivity analysis for each species at 651 nm to reduce the impact of absorption and using the cell size distributions measured at the 15:00 sampling point. We varied the values for the following input parameters: shell refractive index; real part of the refractive index of the core; imaginary part of the refractive index of the core; power exponent of Junge distributions; shell thickness (for the coated spherical model only); cell diameter; and cell numbers. For each parameter, we found realistic maximum, minimum and average values from the literature and made the calculations

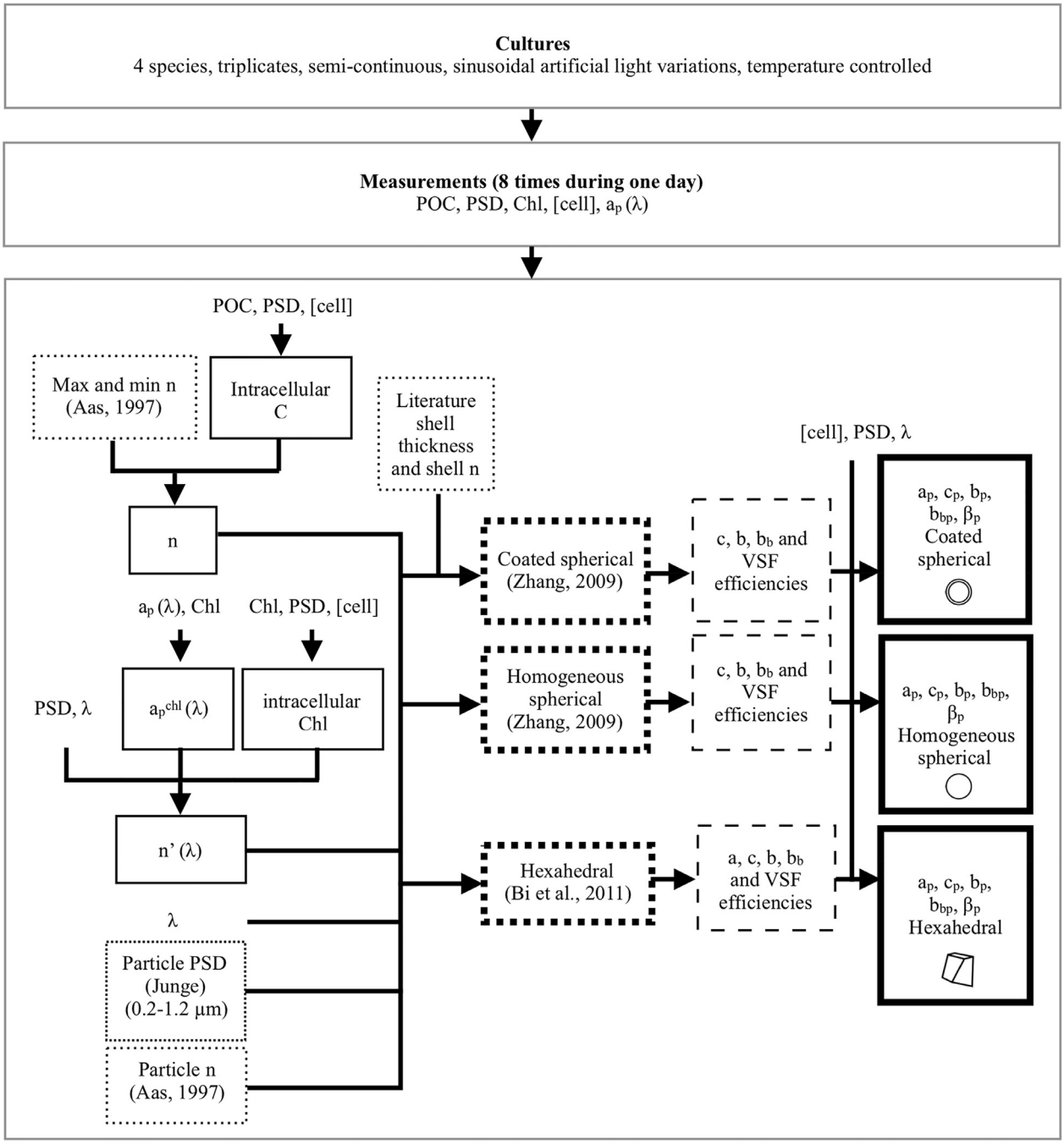

Fig. 2. Flow chart of the models. Model inputs calculated from measurements are in boxes with thin solid lines. Model inputs from literature are in dotted boxes. Models are in thick short-dashed boxes, model direct outputs are in boxes with thin dashed lines and final model IOPs outputs are boxes with thick solid line.

varying only one parameter at a time to examine its influence on b_{bp}/b_p, $\beta_p(124)$, c_p and a_p.

In addition, since the particles with radius smaller than 1.12 µm were not measured by the Coulter Counter, we conducted a sensitivity analysis where we added particles following Junge distributions with their amplitude set by the smallest bin of the Coulter Counter and varied the power law exponents. The particle size distributions were modelled between 0.2 µm to 1.12 µm and their refractive index was assumed to be invariant during the experiment and did not include an imaginary part. The n for these small particles was set at 1.2 (calcite) for *E. huxleyi* [53,72] and 1.058 (representing particles similar in composition to marine bacteria) for the other species [72].

3.2.3. Reproducing diel variations with models

We tested different combinations of the input parameters within their realistic ranges to obtain the closest fit to the measurements for b_{bp}/b_p, $\beta_p(124)$, c_p and a_p for diel variations.

4. Results

4.1. Sensitivity analyses

4.1.1. Overall comparison with measurements

For the coated spherical model (Fig. 3), the ranges of IOP values obtained through the sensitivity analysis overlapped within 1

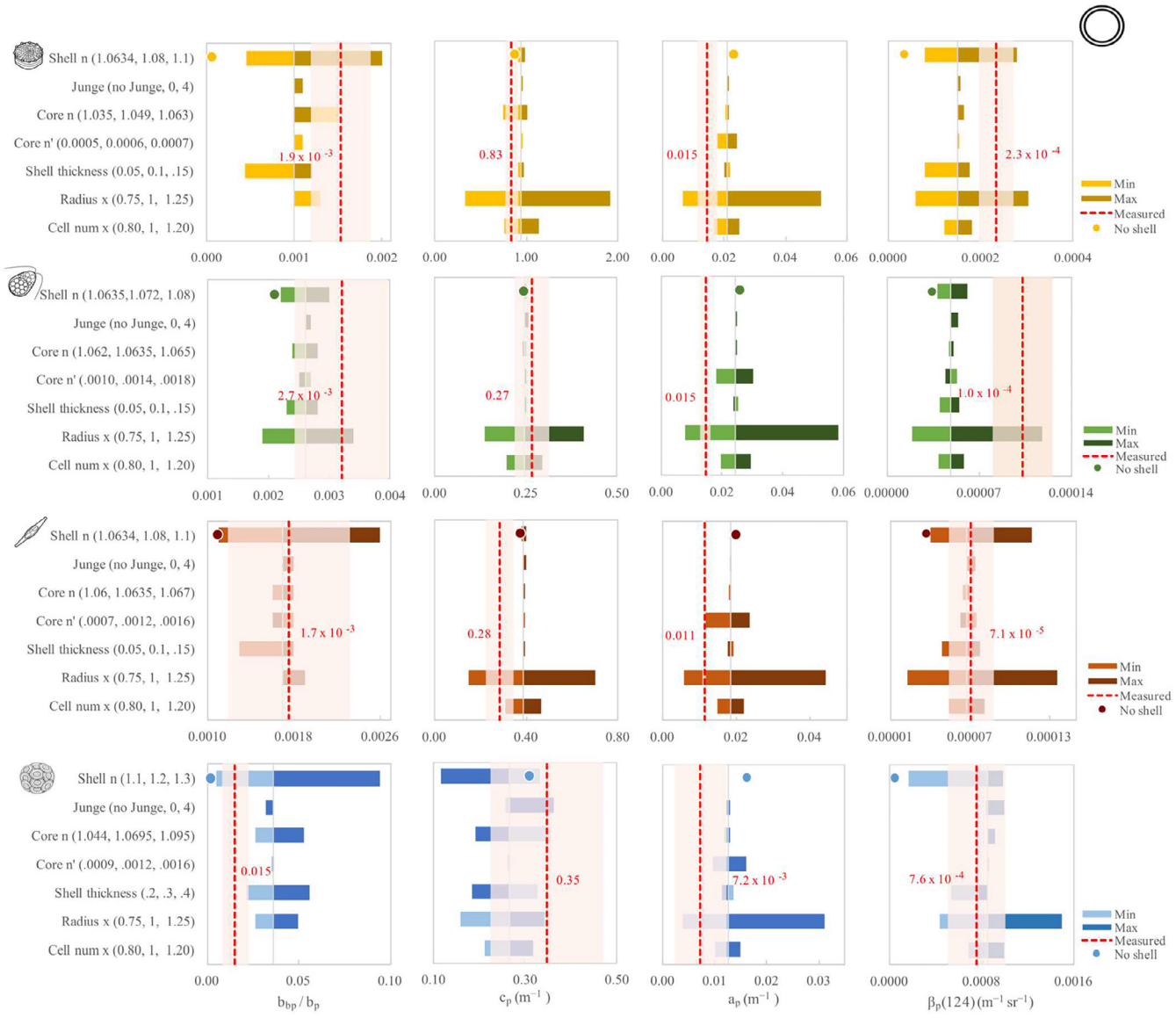

Fig. 3. Sensitivity analysis of our coated spherical particle model for b_{bp}/b_p, c_p, a_p and $\beta_p(124)$ at 651 nm at the 15:00 time point. The homogeneous sphere model with the "average" core n is represented by the filled circle on the 'Shell n' row on each panel. The dashed vertical line indicates the average measurement value while the pink rectangle represents one standard deviation. (For interpretation of the references to color in this figure legend, the reader is referred to the web version of this article.)

standard deviation the measured values (shaded region overlaid on Fig. 3) for all species and IOPs. This shows that the coated spherical model can be used within a reasonable range of input parameters to represent the measured values. The sensitivity analysis results for the homogeneous spherical model only overlapped with the measurements for c_p and a_p, which is consistent with previous observations [35,37,70,71]. The sensitivity analysis results for the hexahedral model (Fig. 4) overlapped with the measurements for c_p and a_p for all species. They also fit the b_{bp}/b_p and $\beta_p(124)$ for *P. tricornutum* and they fit the $\beta_p(124)$ for *E. huxleyi* in rather extreme conditions (n ~1.198). The model results for the hexahedral particles were too low for b_{bp}/b_p and $\beta_p(124)$ of *D. tertiolecta* and *T. pseudonana*. In summary, the hexahedral model generally provided estimates of $\beta_p(124)$ that were too low while the coated spherical model could match all the observations within the realistic ranges of the input values.

4.1.2. Cell radius

A ± 25% variation in cell size was tested because of the difficulty to adequately measure equivalent cell diameter of non-spherical particles with a Coulter Counter [95]. For all models, a 25% difference in cell radius led to significant range of changes (~ −66 to 140% change) on the modelled outputs of a_p, c_p and β_p, and was generally the largest influence on the IOPs among the variables. Its impact was less important on the backscattering ratio (~ −33 to 38% change).

4.1.3. Shell n

For the coated spherical model, the shell's refractive index had an important effect on $\beta_p(124)$ (Fig. 3, from ~ −80 to 80% change). Removal of the shell returns values for $\beta_p(124)$ that are ~10% of the average values for *E. huxleyi*, 25% for *T. pseudonana*, 55% for *P. tricornutum* and 75% for *D. tertiolecta* (compare point with the gray vertical line on Fig. 3). The b_{bp}/b_p is also strongly influenced by the n_{shell} (~ −80 to 160% change) while c_p is not (~ −55 to 25% change for *E. huxleyi*, ~ −4 to 4% change for other species). This is consistent with previous observations by Meyer [65], Quinby-Hunt et al. [66], Kitchen and Zaneveld [34] and Bernard et al. [45]. Witkowski

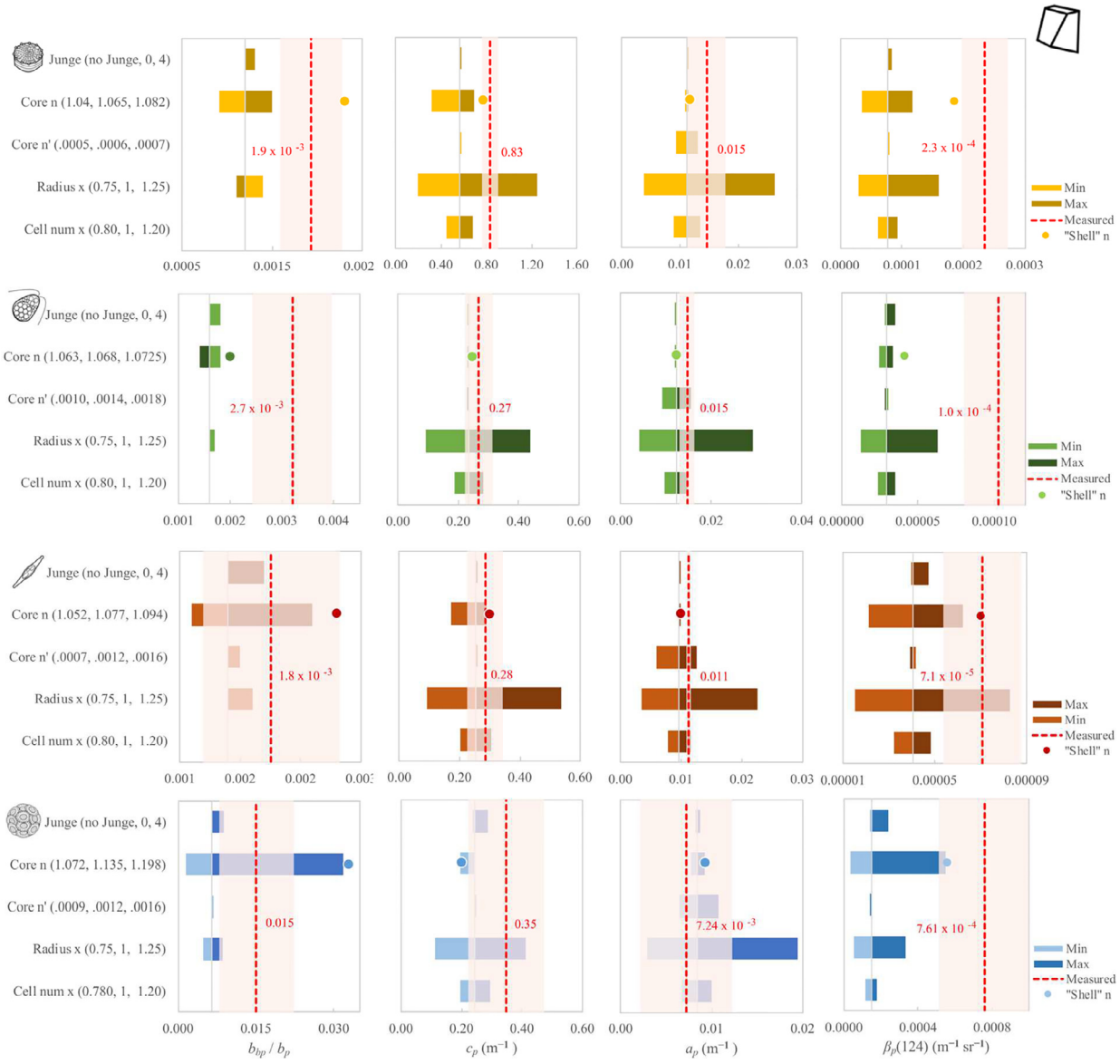

Fig. 4. Sensitivity analysis for the hexahedral particle model for b_{bp}/b_p, c_p and a_p and $\beta_p(124)$ at 15:00 and 651 nm. The filled circle on the 'Core n' row is calculated with the core n at the value of the shell's n (1.08 for *D. tertiolecta*, 1.1 for *T. pseudonana* and *P. tricornutum* and 1.2 for *E. huxleyi*). The dashed vertical line indicates the average measurement value while the pink rectangle represents one standard deviation. (For interpretation of the references to color in this figure legend, the reader is referred to the web version of this article.)

et al. [96,97] also modelled that cell membrane had an influence on scattering.

4.1.4. Shell thickness

Frustule thickness can vary between 0.063 µm and 0.15 µm for *T. pseudonana* [91], calcite layers in coccolithophores vary in average between 0.28 and 0.35 µm, but can be as low as 0.1 µm in cultures [92]. Similarly, when the outer layer is used to represent chloroplasts in some models (e.g., [45,64,67]), its thickness also varies. For example, Janssen et al. [98] found that chloroplasts relative volume to the cell could vary between 4 and 57% in diatoms depending on the growth conditions [45].

We found that the r_{shell} has an important effect on the backscattering ratio and $\beta_p(124)$ (from ~ −47 to 55% change) and almost no effect on c_p,(~ −23 to 30% for *E. huxleyi* and −4 to 4% for others) which is consistent with the models of Meyer [65], Quinby-Hunt et al. [66] and Kitchen and Zaneveld [34].

4.1.5. Small particles

We tested the effect of small particles by adding a Junge distribution with a power exponent up to 4 (see methods). For the coated spherical models, the effect of those small particles on all the modeled IOPs was relatively small (~ −4 to 36%) compared to the effect of shell refractive index and radius.

4.1.6. Core n and n'

Relative to other input parameters, the core *n* affects b_{bp}/b_p more than the other IOPs for both the spherical and hexahedral models. For the hexahedral model, the core *n* has an important effect (~ −75 to 387% for *E. huxleyi*, ~ −50 to 62% for other species). Kitchen and Zaneveld [34] found a larger effect of variations of the refractive index between 1.02 and 1.09 on attenuation and scattering for homogenous spheres models; the range they examined is, however, much larger than what we used here.

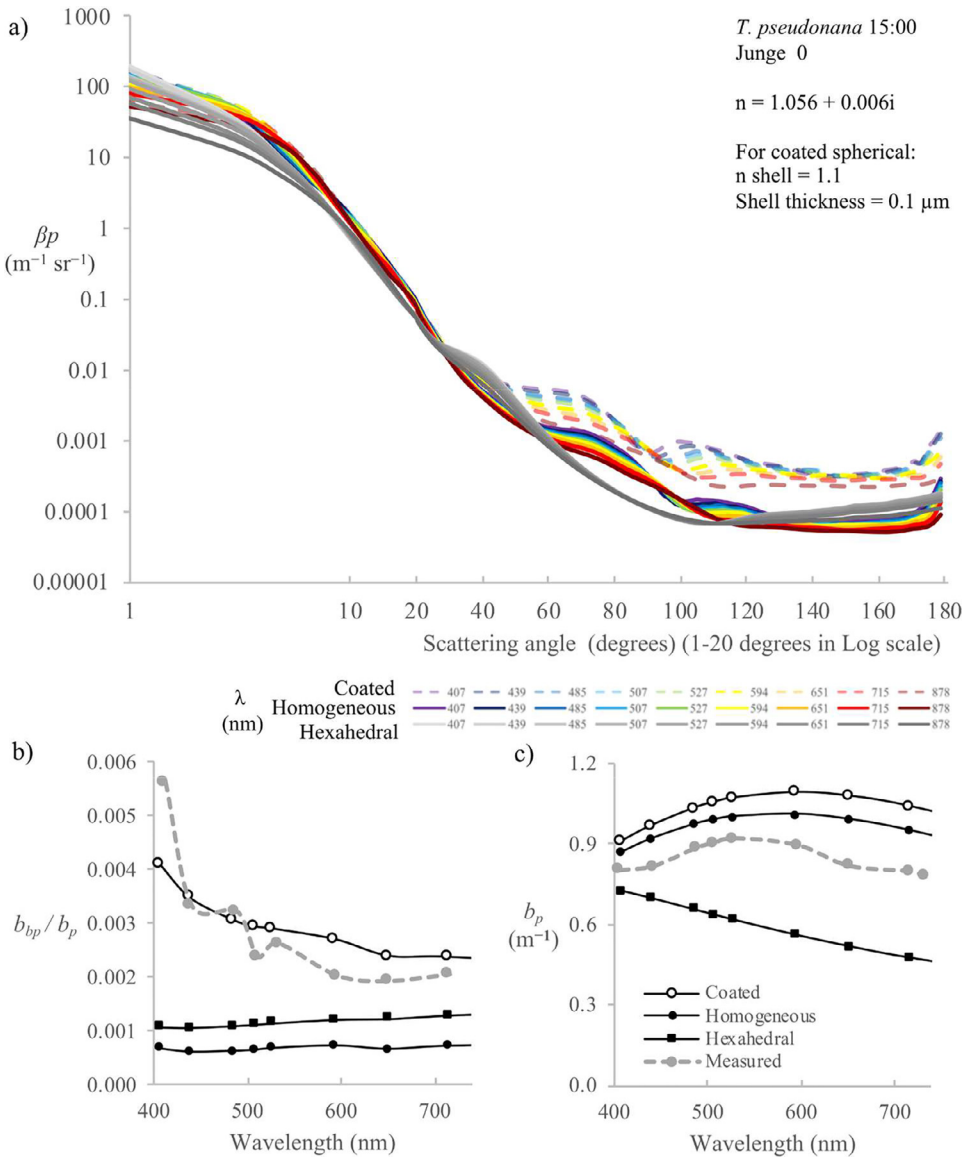

Fig. 5. a) Comparison of the volume scattering functions obtained by the hexahedral (gray), homogeneous spherical (solid colored lines) and coated spherical (dashed colored lines) models for *T. pseudonana* at 15:00 with $n_{shell} = 1.1$, $r_{shell} = 0.1\,\mu m$ and a population of particles smaller than a radius of 1.12 µm represented by a Junge distribution of slope 0. Angles from 1 to 20° are displayed on a logarithmic scale and those from 20 to 180° are on a linear scale. The same cell size distribution was used for all models. b) Spectra of b_{bp}/b_p and c) spectra of b_p for the three models and measurements for the same samples and inputs.

4.1.7. Cell number

We tested the effect of a 20% variation in cell numbers, representing the uncertainty in our Coulter Counter counts for the same culture at the same time. This has theoretically no effect on the backscattering ratio, its 20% effect on the other IOPs was less important than the shell's characteristics on $\beta_p(124)$ (~ -20 to 20% change) and less important than the shell radius for c_p and a_p (~ -20 to 20% change).

4.1.8. Shape

The differences between different modelled shapes for β_p are more pronounced between 60 and 120° where the spherical model is higher than the hexahedral model (Fig. 5a). We found that the effect of adding a shell to the homogeneous spherical model had a more important effect than the shape of the particles for b_{bp}/b_p; the values of the homogenous models were within 45% of each other while adding a shell increased b_{bp}/b_p by 300% to values within 35% of the measurement (Fig. 5). For b_p, the two spherical models were more similar to each other and closer to the measurements (within 22%) while the hexahedral model was up to 70% lower. This is consistent with Volten et al. [99] and Quinby-Hunt et al. [66] finding that internal structures played a more important role in scattering than shape. The shape has an influence on the b_p's spectrum, the spherical models seem to represent both the amplitude and shape of the spectrum better for the tested case. Our results are similar to those of Quirantes and Bernard [37] and Clavano et al. [39] that showed that absorption and attenuation were not strongly influenced by the particle shape in scattering models of off-centered coated spherical and randomly oriented spheroid models.

The modeled b_{bp}/b_p spectrum (Fig. 5b) of the coated spherical model showed decreasing values with wavelengths that were close to the measurements, even though the blue head of the ECO BB9 gave noisier results. The b_p spectra (Fig. 5c) seem to show that total scattering is more affected by shape than coating with the hexahedral model showing values that are ~40% lower than both

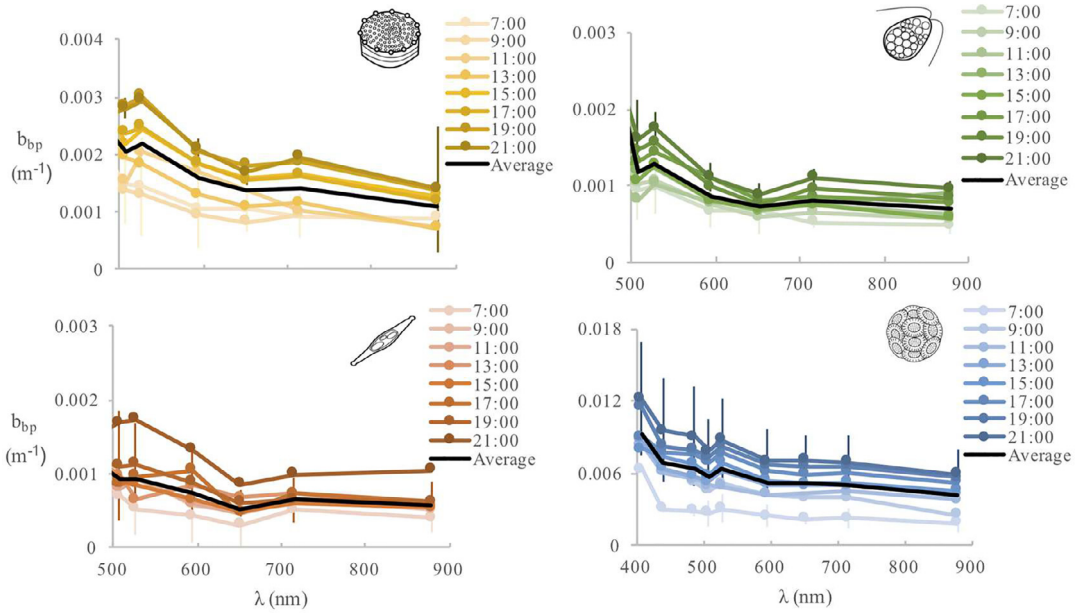

Fig. 6. Average b_{bp} spectra measured at the different times of the day and their daily average spectra for *T. pseudonana, D. tertiolecta, P. tricornutum* and *E. huxleyi*. Error bars show the standard deviations between the culture replicates.

spherical and coated spherical models. Our measured b_{bp} spectra (Fig. 6) are similar to Whitmire et al.'s [41] with a minimum around 630 nm and an increase near 700 nm; they were also made with the same instrument.

4.2. Diel variations

For all species, a reasonable fit of the diel variations of the IOPs was obtained with a Junge slope of 0 and the coated spherical model, suggesting that particles of radii from 0.2 to 1.12 µm did not have an important contribution to the IOPs measured, as expected from the sensitivity analysis.

4.2.1. T. pseudonana

For *T. pseudonana* (Fig. 7), the hexahedral and homogeneous spherical model had an acceptable fit for both a_p and c_p, but were too low for $\beta_p(124)$ and b_{bp}/b_p, as expected [35,37,70,71]. The coated spherical model had the best fit to all the measurements. It exceeded the measurements mostly at the last time point of the day; since this species possesses a silica frustule and has a cylindrical shape of a low elongation ratio, the coated spherical model is also intuitively the most appropriate of the model tested.

4.2.2. D. tertiolecta

For *D. tertiolecta* (Fig. 8), the hexahedral model gives a good fit for c_p and a_p only, and is too low for $\beta_p(124)$ and b_{bp}/b_p. The homogeneous spherical model gives higher values, but the fit for $\beta_p(124)$ and b_{bp}/b_p is still poor. The coated spherical model gives a closer fit than the others, but still gives values that are slightly too low for $\beta_p(124)$ and b_{bp}/b_p, especially for the shorter wavelengths and too high for c_p; the $\beta_p(124)$ is also inverted. It is possible that this species' complex internal structure is harder to simulate using the coated sphere with a homogeneous "soft" interior.

4.2.3. P. tricornutum

Of the species examined here, the hexahedral model had the closest fit for *P. tricornutum* (Fig. 9). The modelled values of $\beta_p(124)$ and b_{bp}/b_p were nevertheless underestimated. The homogeneous spherical model gave a good fit for a_p, but slightly overestimated c_p and was lower than the hexahedral model for $\beta_p(124)$ and b_{bp}/b_p. However, the homogeneous model with the averaged shell and core n that is used for the hexahedral model (not shown) gives higher $\beta_p(124)$ and b_{bp}/b_p values than the hexahedral model. The coated spherical model gave a good fit for all the measurements, but it slightly overestimates c_p. Since this species has a silica frustule, it is logical that the coated model would represent it better. The shape is, however, closer to a hexahedral shape than a sphere, so models using a hexahedral model with coating or an elongated spheroid with shell (e.g., [37]) should be evaluated.

4.2.4. E. huxleyi

For *E. huxleyi* (Fig. 10), the hexahedral model was too low for all the measurements, though the estimates for a_p and c_p are fairly close (within 50%). The homogeneous spherical model gave better results only for a_p, but the homogeneous spherical model with the averaged shell and core n (not shown) gave better results than the hexahedral model for $\beta_p(124)$ and b_{bp}/b_p. The coated spherical model provided a particularly precise estimate for a_p. The last part of the day was lower than the averages of the measurements, but still inside the standard deviations for c_p and b_{bp}/b_p was also inside the standard deviations. The $\beta_p(124)$ was underestimated for the last part of the day. *E. huxleyi* is a spherical coccolithophore covered with calcite coccoliths. While a calcite coating is a reasonable approximation of that layer of coccoliths, it is possible that the more complex structures in it play a role in the differences we see between the model and the measurements. Still, the importance of the calcite shell in models has been demonstrated before [44,100].

Even if the core's refractive index was changed throughout the day to represent carbon accumulation in the cell, the shape of the models' diel variations for c_p, a_p, $\beta_p(124)$ was more strongly influenced by the changes in cell concentration (see Fig. 1a).

4.2.5. Cross-sections for c_p and $\beta_p(124)$

The IOPs presented above are equivalent to those measured in the field. Interpretation of their diel cycles in the field are generally interpreted in term of biomass. Laboratory measurements allow us to remove the effect of changes in the cellular concentration by examining the diel variations in cross-sections thereby

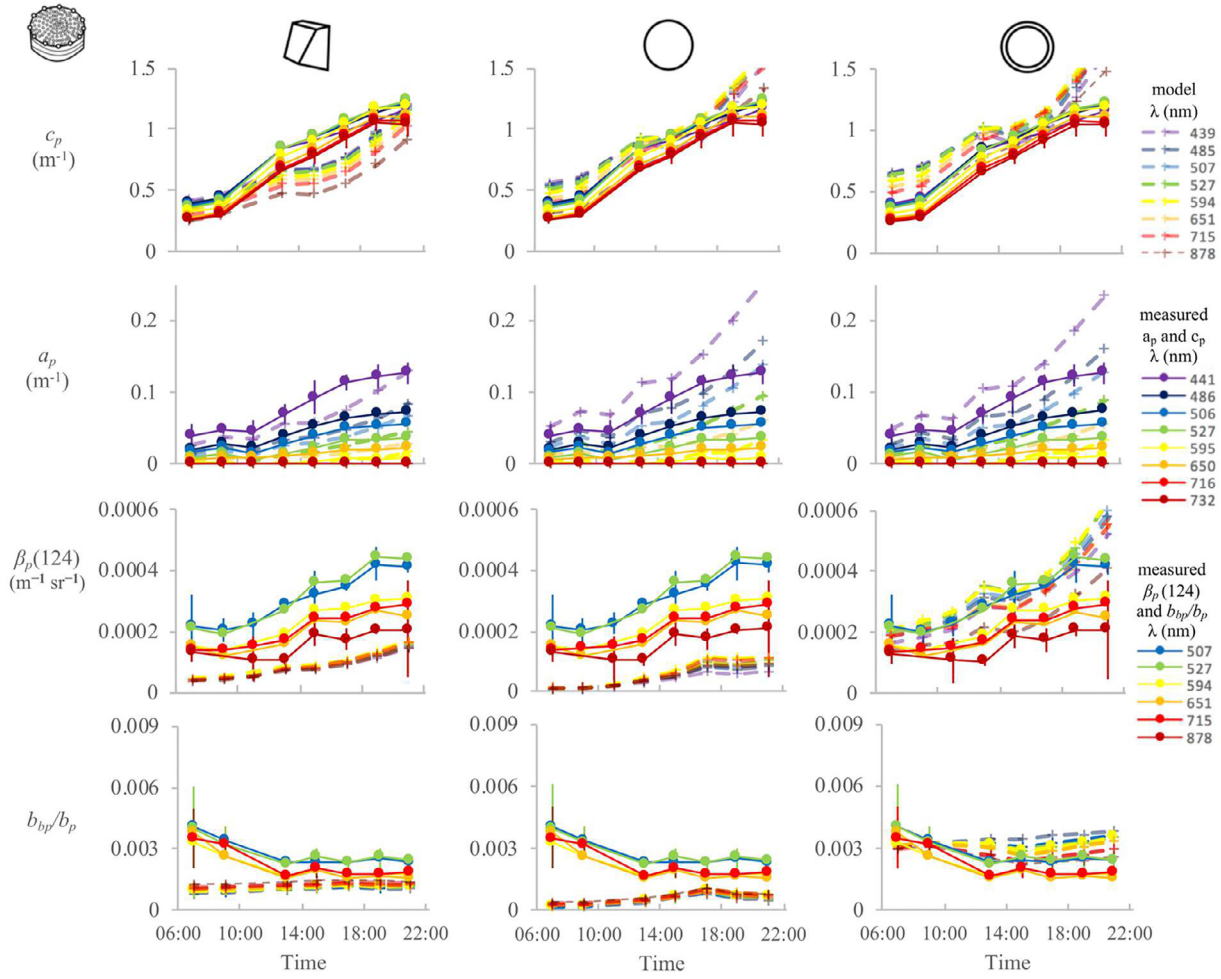

Fig. 7. Diel variations of c_p, a_p, $\beta_p(124)$ and b_{bp}/b_p for the measurements (full lines) and hexahedral, homogeneous spherical and coated spherical models (dashed) for *T. pseudonana*. Inputs for the models shown are a Junge slope of 0 and an n of 1.058 for particles of a radius smaller than 1.12 µm, a r_{shell} of 0.1 µm, n_{shell} of 1.1 for the coated spherical model, a core n that varies according to carbon concentration (averaged with the shell's n for the hexahedral model). Errors bars represent the standard deviations of the measurements for the shortest and longest wavelengths shown.

looking only at in cell-specific changes. When computing cross-sections, the model outputs are only a function of: the cell diameter; the real part of the refractive index; and imaginary part of the refractive index. We can further expect that shape and internal structure would play a role in the measurements.

Attenuation cross-sections (Fig. 11; σ_c, m^2 cell^{-1}) were well modeled by the hexahedral model for *P. tricornutum* and *D. tertiolecta*, which are the least spherical cells in this study. The spherical models overestimated σ_c for the second half of the day. *D. tertiolecta* and *P. tricornutum* were better modeled by the hexahedral model than the coated spherical model for σ_c, which is less affected by the shell [35,37,70,71]. There are significant differences between the measurements and the models for σ_c, indicating that there are intracellular diel changes that are not well represented by our models. It is possible that there are diel changes in the thickness of the shells, as observed by Moutier et al. [101], or even its refractive index. The spectral shape (i.e. positive or negative slope with wavelength) tended to be well represented by the model for *T. pseudonana* and *D. tertiolecta*. The models consistently had the spectral slope inverted with respect to the measured spectra for *P. tricornutum* and *E. huxleyi*.

The $\beta_p(124)$ cross-sections ($\sigma_{\beta p(124)}$, m^2 cell^{-1}) were underestimated by the hexahedral and the homogeneous sphere model for all species (Fig. 12), the modeled spectral shapes where also much flatter than the measurements. The coated sphere model provided values that were in the right range, but the model values showed more diel variations than the measurements and spectral shapes were only reproduced for some species. *E. huxleyi*, was an exception with respect to diel changes where the measurements of $\sigma_{\beta p(124)}$ show an overall increase of ~50% during the day that was not reproduced by the models. These results suggest that we overestimated the diel variations in core refractive index in the models by assuming that they would span the range of measured values within 1 day, since it is the only factor that varied with time other than cell numbers and size, which we measured. Alternatively, it could be that smaller particles play a larger role than modelled here and would reduce the overall diel changes observed.

We correlated the IOPs cross sections with carbon (*C*) and chlorophyll (*Chl*) per cell, as well as the cell diameter (Table 1). We consider a correlation strong when the coefficient of determination is greater than 0.5 and weak when it is between 0.25 and 0.5, while we consider that there is essentially no correlation below 0.25. The $\sigma_a(677)$ correlated strongly with *C* and *Chl* per cell for *T. pseudonana* and *D. tertiolecta*. The latter also had a strong correlation of $\sigma_a(677)$ with cell diameter. $\sigma_a(677)$ had only weak correlations with *C* and *Chl* per cell for *P. tricornutum* and no correlations with any of the factors for *E. huxleyi*. The $\sigma_c(715)$ correlates with *C* and *Chl* per cell for *T. pseudonana* and only *C/cell* for

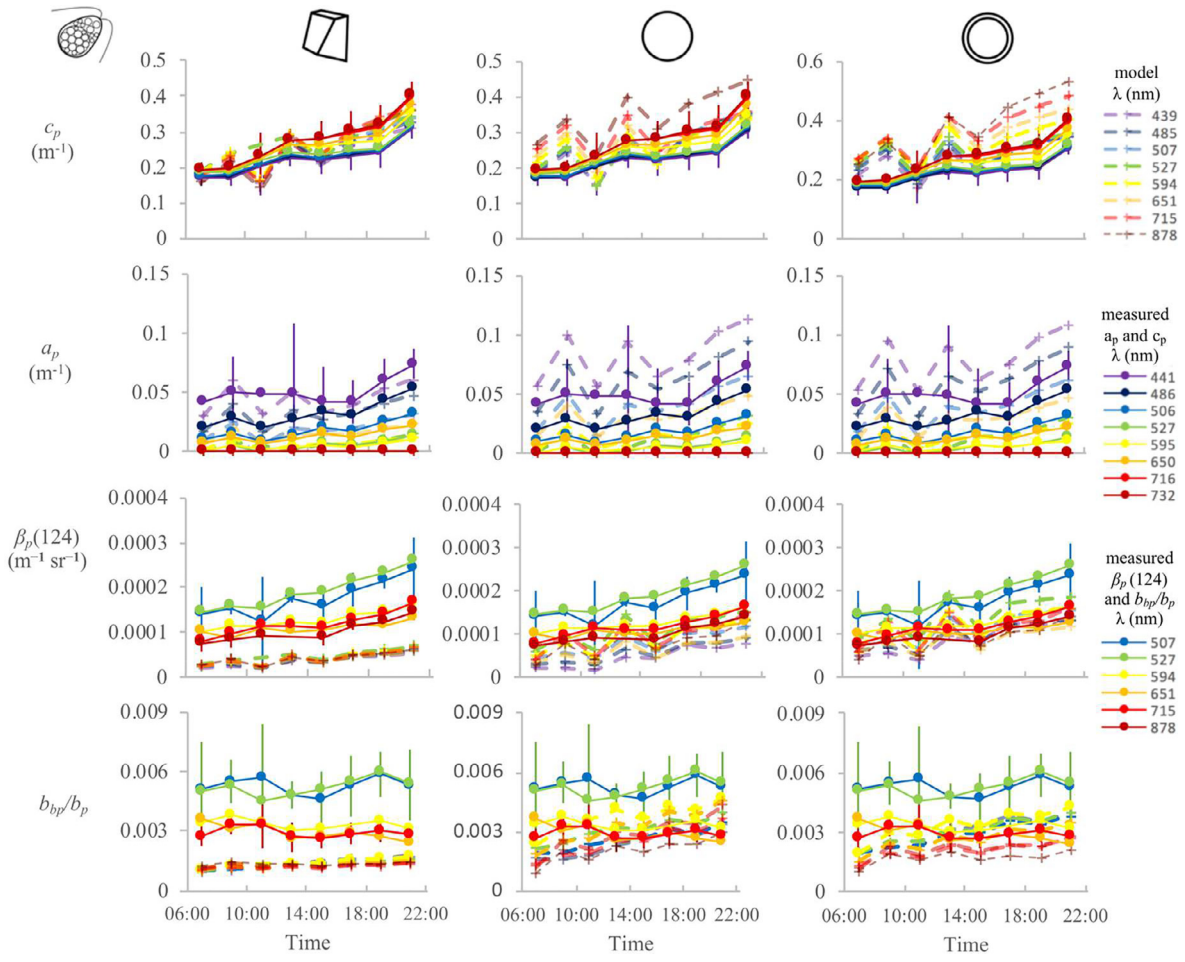

Fig. 8. Diel variations of c_p, a_p, $\beta_p(124)$ and b_{bp}/b_p for the measurements (full lines) and hexahedral, homogeneous spherical and coated spherical models (dashed) for *D. tertiolecta*. Inputs for the models shown are a Junge slope of 0 and a n of 1.058 for particles of a radius smaller than 1.12 µm, r_{shell} of 0.1 µm, n_{shell} of 1.08 for the coated spherical model, a core n that varies according to carbon concentration (averaged with the shell's n for the hexahedral model). Errors bars represent the standard deviations of the measurements for the shortest and longest wavelengths shown.

Table 1
Coefficients of determination (r^2) of $\sigma_a(715)$ (m^2·cell^{-1}), $\sigma_c(715)$ (m^2·cell^{-1}) and $\sigma_{bb}(715)$ (m^2·cell^{-1}) (to avoid the effect of absorption) with intracellular carbon content (*C*/cell, µg·cell^{-1}), intracellular *Chl* concentration (µg·cell^{-1}) and cell diameter (µm). Coefficients of determination larger than 0.50 are in bold font and those between 0.25 and 0.5 are underlined.

		C/cell	*Chl*/cell	diameter
T. pseudonana	$\sigma_a(677)$	**0.57**	**0.77**	0.31
	$\sigma_c(715)$	**0.89**	**0.54**	0.37
	$\sigma_{bb}(715)$	0.09	0.15	0.02
D. tertiolecta	$\sigma_a(677)$	**0.52**	**0.70**	**0.68**
	$\sigma_c(715)$	0.27	**0.71**	0.45
	$\sigma_{bb}(715)$	0.15	**0.54**	0.17
P. tricornutum	$\sigma_a(677)$	0.44	0.46	0.26
	$\sigma_c(715)$	**0.79**	**0.70**	0.29
	$\sigma_{bb}(715)$	0.00	0.06	0.06
E. huxleyi	$\sigma_a(677)$	0.10	0.23	0.00
	$\sigma_c(715)$	**0.71**	0.20	0.27
	$\sigma_{bb}(715)$	**0.84**	0.45	0.26

E. huxleyi. It also correlated with *C* and *Chl* per cell for *P. tricornutum*. The backscattering cross section correlates with nothing we tested for the diatoms, but correlates with *Chl/cell* for *D. tertiolecta*. It also correlates with *C/cell* for *E. huxleyi*. The cell diameter had weak correlations with σ_c and showed no correlation with σ_{bb} of all species except for a weak correlation for *E. huxleyi*, indicating that it is generally not the factor driving diel changes in the IOPs across different species.

5. Discussion

5.1. Quality of the measurements and calculations

We discussed the quality of our backscattering measurements in Poulin et al. [86]. We took the outmost care to reduce the impact of small particles in our measurements, and the only small particles that could affect the measurements are those that were present in the cultures, that we also were careful to minimize by diluting every day with sterile 0.2 µm filtered culture medium and working in sterile conditions. We did not measure the particles smaller than a radius of 1.12 µm. While they certainly increase slightly the IOPs measured; the sensitivity analysis suggests that this would be a minor impact, (always less than 25%). It is, therefore, unlikely that they would influence the diel variations. Given these observation, we computed most of our modeling comparison with a Junge slope of 0, representing constant particles for all small size, equal to those measured at the smallest bin measured by the Coulter Counter.

The use of the volume-equivalent spherical diameter can also be a source of uncertainty in the model results, especially for the

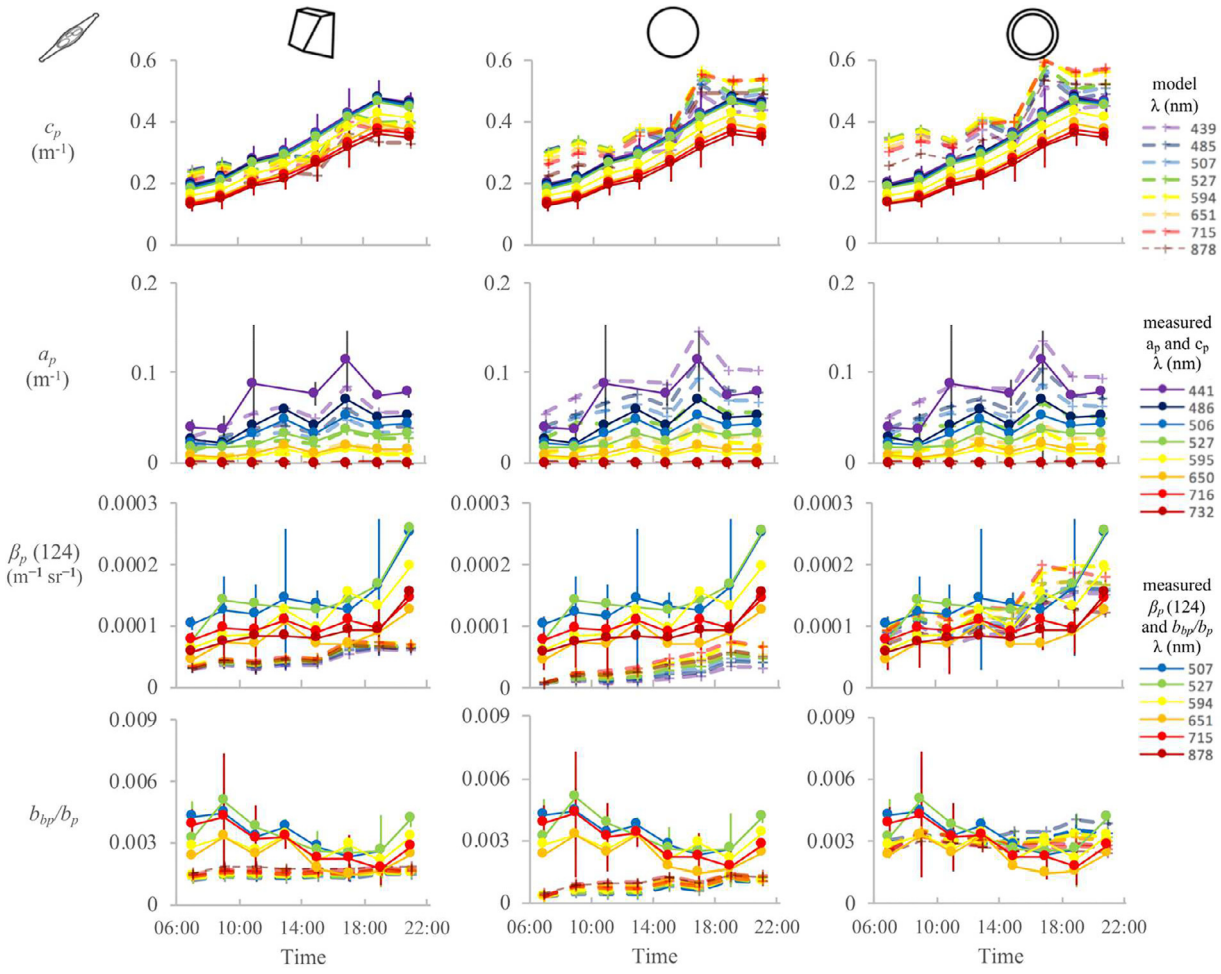

Fig. 9. Diel variations of c_p, a_p, $\beta_p(124)$ and b_{bp}/b_p for the measurements (full lines) and hexahedral, homogeneous spherical and coated spherical models (dashed) for *P. tricornutum*. Inputs for the models shown are a Junge slope of 0 and a n of 1.058 for particles of a radius smaller than 1.12 µm, r_{shell} of 0.1 µm, n_{shell} of 1.1 for the coated spherical model, a core n that varies according to carbon concentration (averaged with the shell's n for the hexahedral model). Errors bars represent the standard deviations of the measurements for the shortest and longest wavelengths shown.

species that are further from the spherical shape, for which it is difficult to find a representative diameter. Another choice could have been area equivalent diameter, which would have resulted, for example, in diameters 90.95% of the volume-equivalent spherical diameter we used if we assumed a cubical shape.

As described in the methodology, the imaginary part of the refractive index was estimated using the measured absorption coefficients. Consequently, the performance of our models depends on the measurements of absorption. This would directly affect the results for absorption, so it is important to take that into account when interpreting our results. It should not have a major impact however, as our sensitivity analyses show that variations in cell size have more impact on modelled absorption than the imaginary part of the refractive index.

5.2. Comparison with literature

Our results showed that homogeneous models can reproduce measurements of attenuation and absorption, but not backscattering, which is consistent with earlier studies [35,37,70,71]. We also observed that a coated spherical model can represent the measurements reasonably, even for backscattering. There have been many modeling studies of the increase of backscattering cross-section with the inclusion of a second or third layer in spherical models [34,37,44,65,66]. We show here that this increase is adequate to represent phytoplankton cells backscattering.

Our sensitivity analyses show that the refractive index of the shell has a large impact on model outputs. Varying its value by an amount comparable to what could be attributed to uncertainty in measurements and its impacts on the backscattering ratio was greater than 25% differences in radius (for the species that possess a shell). The importance of the shell's refractive index on backscattering has been noted before [34,101].

Our findings regarding the impact of shape versus shells is similar to those of Quirantes and Bernard [64] who compared the spheroidal versus the spherical model with and without shells: the inclusion of a shell in the spherical models had more influence on backscattering than the shape of the cells (here asymmetrical hexahedral vs spherical). Total scattering, however, is more influenced by shape.

Diel variations of the IOPs and models show that the variations in cell number have the largest impact on the diel variations of optical properties. However, the attenuation cross-sections and the correlations with absorption and backscattering cross-sections show that diel variations of the measurements are not only due to cell numbers and are affected by cellular structure. Ackleson et al. [102] also found that short term light induced variations of phytoplankton attenuation and cellular scattering were likely indepen-

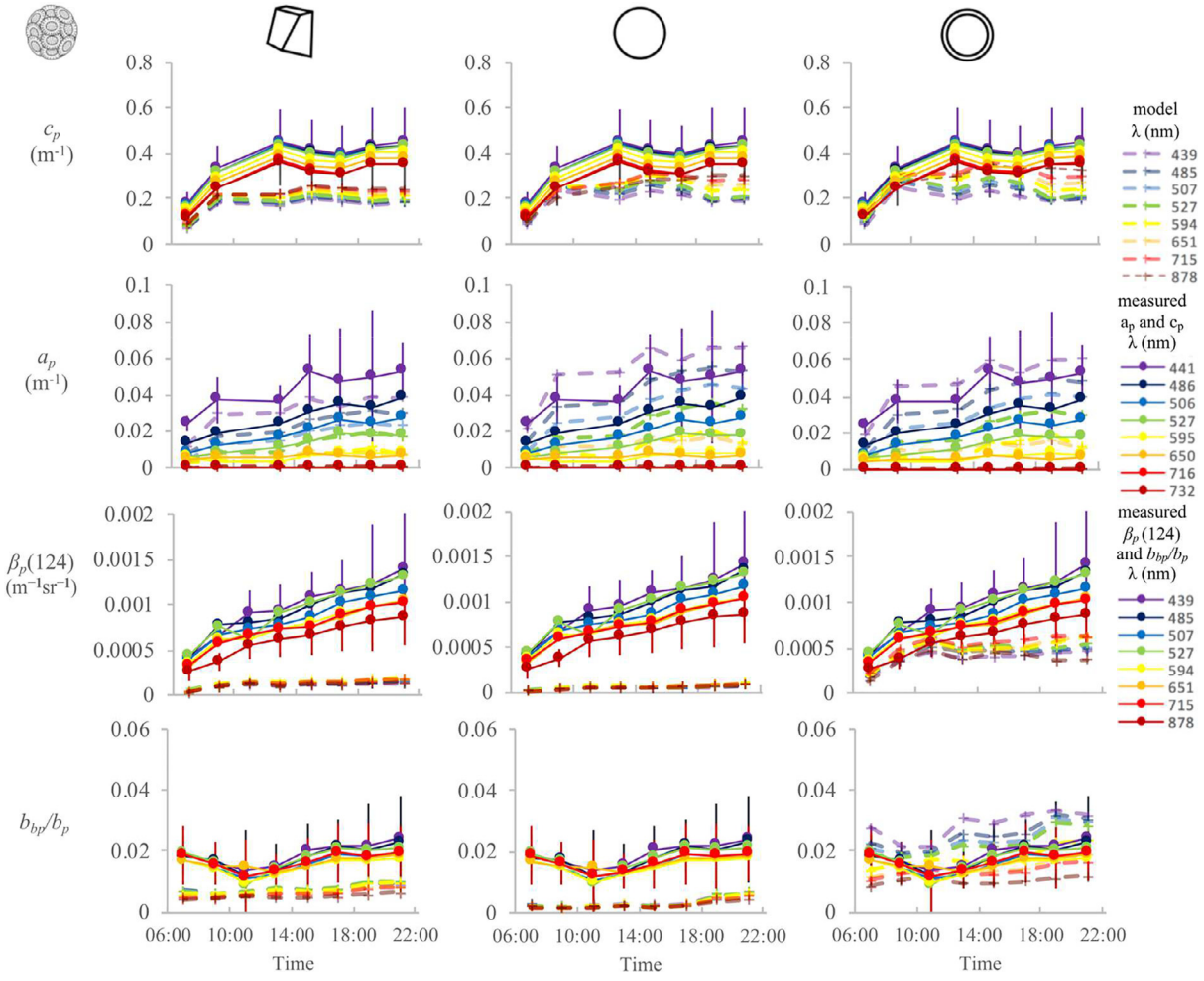

Fig. 10. Diel variations of c_p, a_p, $\beta_p(124)$ and b_{bp}/b_p for the measurements (full lines) and hexahedral, homogeneous spherical and coated spherical models (dashed) for *E. huxleyi*. Inputs for the models shown are a Junge slope of 0 and a n of 1.2 for particles of a radius smaller than 1.12 µm, r_{shell} of 0.1 µm, n_{shell} of 1.2 for the coated spherical model, a core n that varies according to carbon concentration (averaged with the shell's n for the hexahedral model). Errors bars represent the standard deviations of the measurements for the shortest and longest wavelengths shown.

dent of biomass and more influenced by cellular structure. The cell structures were not modeled herein, even if the values obtained by the models are close to the measurements for the most part. The inclusion of a shell with a refractive index representative of silica or calcite gave good results for the species that possess those shells. Other studies represented chloroplasts as an outer layer in models, and the inclusion of a shell does increase backscattering, but our results show that a refractive index representative of chloroplasts (between 1.02 and 1.06 in Aas [72]) is too low to reach the level of the measurements. Also, Svensen et al. [103] found that a mutant of *Chlamydomonas reinhardtii* that does not possess a cell wall scatters significantly less than the regular strain that has a cell wall, indicating that outer layers of model could be better represented by refractive indices and thicknesses that represent the cell wall instead of the chloroplasts. The correlations we observed could also indicate this; the diatoms' backscattering cross-sections do not correlate with any of our measurements (Carbon, *Chl* and cell size). Perhaps it is more correlated with shell characteristics. Also, while diel variations of frustules have not been studied, Moutier et al. [101] found that frustule thickness varies depending on the growth phase; this would change during the day for synchronized or partially synchronized populations. *E. huxleyi* does show a correlation between the backscattering cross-section and carbon. We removed the calcite by decarbonating our POC samples, but it is possible that a significant part of *E. huxleyi*'s intracellular carbon was in the process of becoming calcite [104] and correlates with backscattering. Also, for *D. tertiolecta*, which does not possess a shell, the backscattering cross section correlates with the number of cells and intracellular chlorophyll. This and the fact that the model including a shell gave better results than the homogeneous spheres could mean that for that species, chloroplasts or other internal structures could be treated as an outer layer in models, like Moutier et al. [101] and Bernard et al. [45] did. Possible improvements to the models could include diel variations in frustule or coccolith thickness and/or refractive index. More research would be needed to understand those variations.

5.3. Implications

We showed that spherical models can fit the measurements of backscattering when a shell is included, and that in cultures, an important amount of backscattering due to small particles is not necessary to obtain closure. This agrees with the conclusions of Vaillancourt et al. [38], Dall' Olmo et al. [46], Whitmire et al. [41] and Martinez-Vicente et al. [47] and who found that phytoplankton could be responsible for more backscattering than previously thought. However, in our simulation of small particles we did not include those of sizes that are in the "dissolved domain", i.e.,

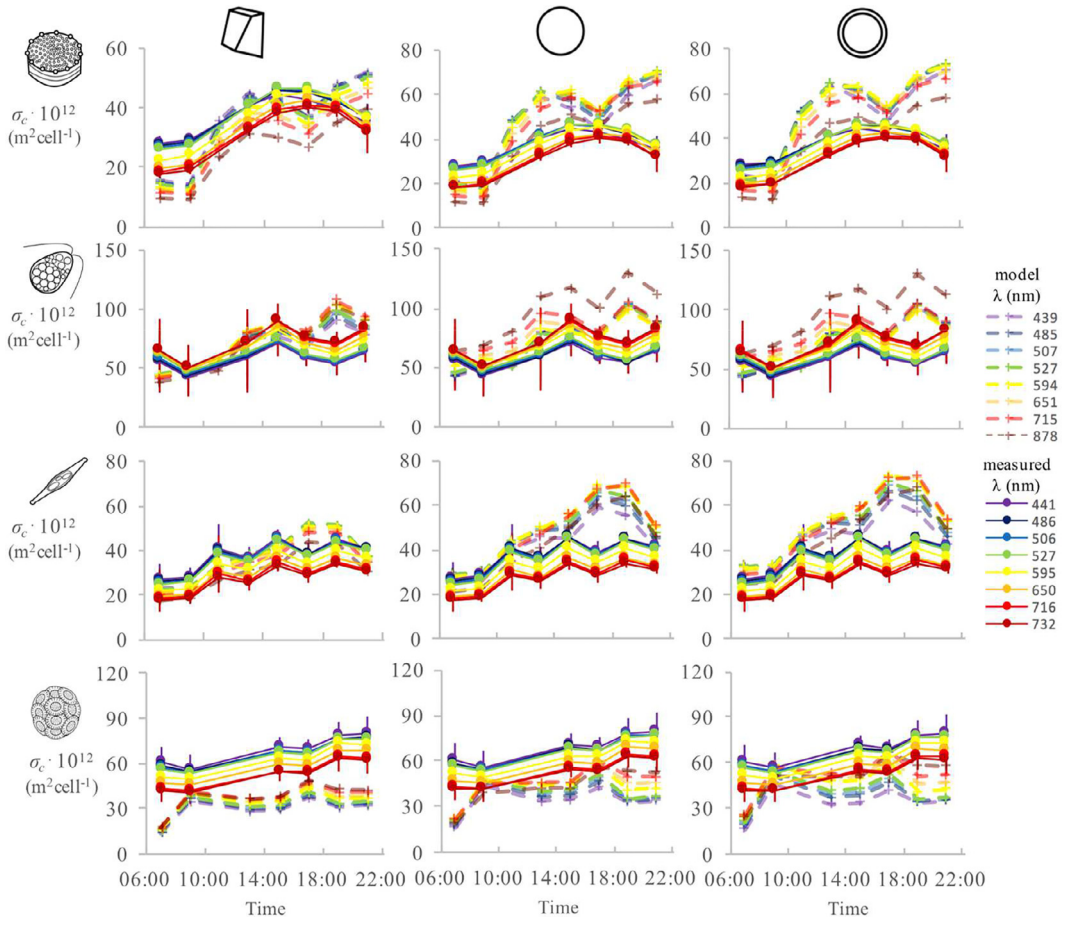

Fig. 11. Diel variations the attenuation cross-section (σ_c) for the measurements (full lines) and hexahedral, homogeneous spherical and coated spherical models (dashed). Errors bars represent the standard deviations of the measurements for the shortest and longest wavelengths shown.

of diameter $< 0.2\,\mu$m because we believe in our controlled experiment the existence of these very small particles is limited. Also, we found that if the Junge distribution has a slope of 5 for particles of sizes 0.2–1.12 µm, which would be unrealistic in our laboratory measurements, but can occur in some cases in the ocean, the small particles would exert a same range of the effect as the shell properties or 25% change in cell radius. Flow cytometry to study the scattering of phytoplankton (e.g. [67,101,102,105–108]) independently from other particles, would provide a complementary information to this study. Again, though, the model used to invert the flow cytometry measurements will have to be carefully chosen.

The hexahedral model that we used could possibly be improved by including a shell. It could be proven useful in populations where the non-sphericity of the phytoplankton is known. However, the simplicity of calculation of the coated spherical model is an advantage and it would be necessary to prove the superiority of the coated hexahedral model to make it worth using routinely. The randomly oriented spheroid model (e.g., [37]) that reduces the 'rainbow effects' associated with perfect spheres may also provide an intermediate level of complexity/computational burden and may be interesting for some applications.

6. Conclusion

We found that the coated sphere model represented overall results better than the homogeneous sphere and hexahedral models, which can reproduce the measurements for the elongated species that we studied, but underestimate the backscattering of the other species. The small particles that we included to represent calcite coccoliths for *E. huxleyi* or bacteria for the other species, did not make a significant contribution to the optical signals in our cultures. Our results also suggest that the representation of cellular structure is more important than the shape of the modelled particles to reproduce the inherent optical properties, especially for backscattering. The differences between species that we observed show that community structure must be considered when studying IOPs. In situ measurements will be necessary to determine if our models can reproduce the diel variations of backscattering that is observed in the ocean.

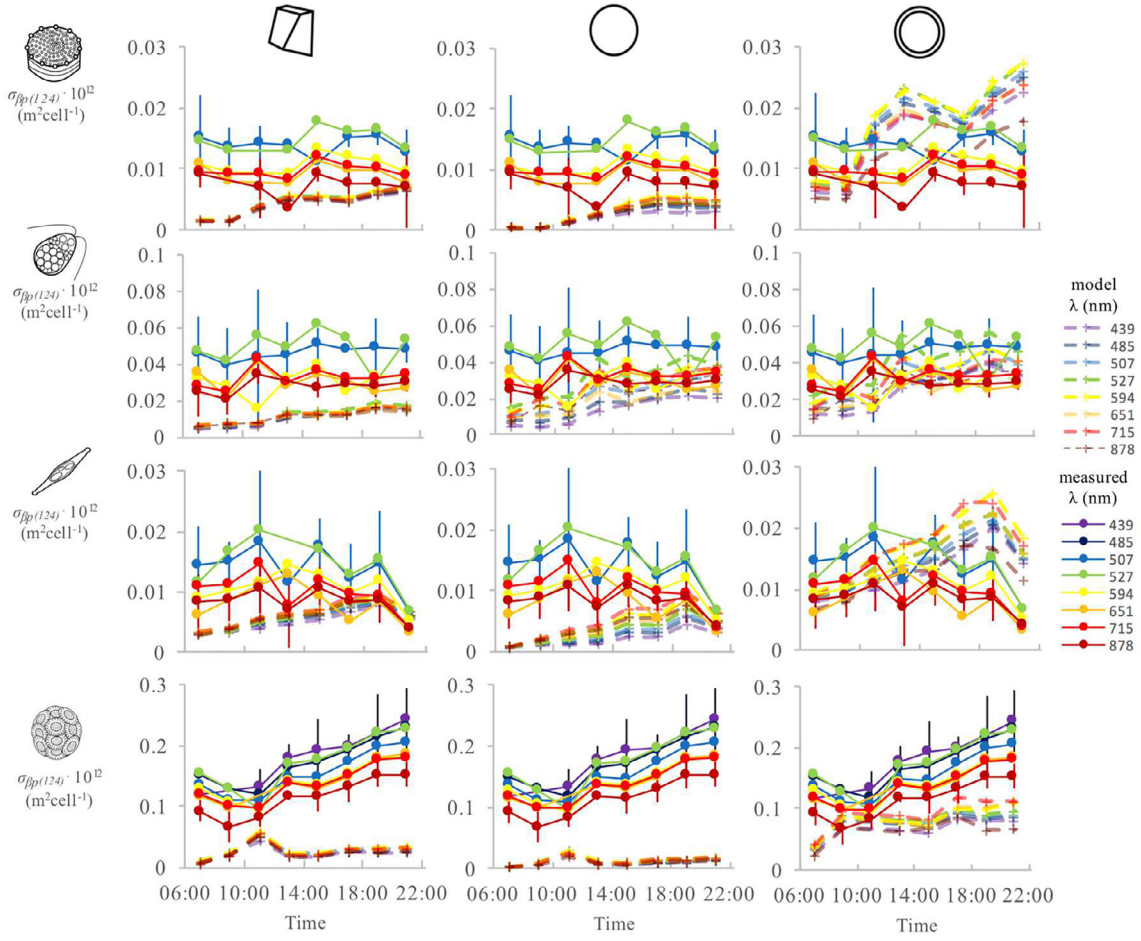

Fig. 12. Diel variations the attenuation cross-section ($\sigma_{\beta p(124)}$) for the measurements (full lines) and hexahedral, homogeneous spherical and coated spherical models (dashed). Errors bars represent the standard deviations of the measurements for the shortest and longest wavelengths shown.

Acknowledgments

We thank an anonymous reviewer and Dr. Steve Ackleson for their helpful and constructive criticism of this article. We thank Gabriel Diab, Pascale Roy, Tara Tapics, Simon Meilleur-Lacasse, Dr. Jennifer Marie-Rose Vandenhecke, Patrick Cliche, Dominic Bélanger, Dominique Marie and Marieke Beaulieu for their invaluable help before and during the experiments.

We are grateful to Dr. Emmanuel Boss for loaning the ac-s and ECO BB9 used and comments.

Thanks to Dr. Darius Stramski, Dr. Mike Twardowski, Dr. David Antoine and Dr. Malika Kheireddine for their comments on earlier versions of this work.

The FRQNT, NSERC and Canada Research Chair program funded this research.

XZ's work was supported by NASA [NNX13AN72G, NNX15AC85G] and NSF [1458962].

PY acknowledges support by the U.S. National Science Foundation under Grant OCE-1459180.

References

[1] Field CB, Behrenfeld MJ, Randerson JT, Falkowski P. Primary production of the biosphere: integrating terrestrial and oceanic components. Science 1998;281:237–40.

[2] Gordon HR, Brown OB, Evans RH, Brown JW, Smith RC, Baker KS, Clark DK. A semianalytic radiance model of ocean color. J Geophys Res Atmos 1988;93(D9):10909–24.

[3] Morel A. Optical modeling of the upper ocean in relation to its biogenous matter content (case I waters). J Geophys Res Oceans 1988;93(C9):10749–68.

[4] Morel A, Antoine D, Gentili B. Bidirectional reflectance of oceanic waters: accounting for raman emission and varying particle scattering phase function. Appl Opt 2002;41(30):6289–306.

[5] Siegel DA, Dickey TD, Washburn L, Hamilton MK, Mitchell BG. Optical determination of particulate abundance and production variations in the oligotrophic ocean. Deep Sea Res Part A. Oceanogr Res Pap 1989;36(2):211–22.

[6] Cullen JJ, Lewis MR, Davis CO, Barber RT. Photosynthetic characteristics and estimated growth rates indicate grazing is the proximate control of primary production in the equatorial Pacific. J Geophys Res Oceans 1992;97(C1):639–54.

[7] Stramska M, Dickey TD. Variability of bio-optical properties of the upper ocean associated with diel cycles in phytoplankton population. J Geophys Res Oceans 1992;97(C11):17873–87.

[8] Gardner WD, Walsh ID, Richardson MJ. Biophysical forcing of particle production and distribution during a spring bloom in the North Atlantic. Deep Sea Res Part II Top Stud Oceanogr 1993;40:171–95.

[9] Bishop JK, Calvert SE, Soon MY. Spatial and temporal variability of POC in the northeast subarctic pacific. Deep Sea Res Part II Top Stud Oceanogr 1999;46(11):2699–733.

[10] Claustre H, Morel A, Babin M, Cailliau C, Marie D, Marty J-C, Tailliez D, Vaulot D. Variability in particle attenuation and chlorophyll fluorescence in the tropical pacific: scales, patterns, and biogeochemical implications. J Geophys Res Oceans 1999;104:3401–22.

[11] Gardner WD, Gundersen JS, Richardson MJ, Walsh ID. The role of seasonal and diel changes in mixed-layer depth on carbon and chlorophyll distributions in the Arabian Sea. Deep Sea Res Part II Top Stud Oceanogr 1999;46(8):1833–58.

[12] Behrenfeld MJ, Boss E. The beam attenuation to chlorophyll ratio: an optical index of phytoplankton physiology in the surface ocean? Deep Sea Res Part I Oceanogr Res Pap 2003;50(12):1537–49.

[13] Gernez P, Antoine D, Huot Y. Diel cycles of the particulate beam attenuation coefficient under varying trophic conditions in the northwestern Mediterranean Ssea: observations and modeling. Limnol Oceanogr 2011;56(1):17–36.

[14] Durand MD, Olson RJ. Contributions of phytoplankton light scattering and cell concentration changes to diel variations in beam attenuation in the equatorial Pacific from flow cytometric measurements of pico-, ultra-and nanoplankton. Deep Sea Res Part II Top Stud Oceanogr 1996;43(4–6):891–906.

[15] Claustre H, Huot Y, Obernosterer I, Gentili B, Tailliez D, Lewis M. Gross com-

munity production and metabolic balance in the South Pacific Gyre, using a non intrusive bio-optical method. Biogeosciences 2008;4(5):463–74.
[16] Kheireddine M, Antoine D. Diel variability of the beam attenuation and backscattering coefficients in the northwestern Mediterranean Sea (BOUSSOLE site). J Geophys Res Oceans 2014;119(8):5465–82.
[17] Vaulot D, Marie D. Diel variability of photosynthetic picoplankton in the equatorial pacific. J Geophys Res Oceans 1999;104(C2):3297–310.
[18] Sosik HM, Olson RJ, Neubert MG, Shalapyonok A, Solow AR. Growth rates of coastal phytoplankton from time-series measurements with a submersible flow cytometer. Limnol Oceanogr 2003;48(5):1756–65.
[19] Preisendorfer RW. Hydrologic optics. vol I. Introduction. US Department of Commerce, National Oceanic and Atmospheric Administration. Environment Research Laboratory; 1976.
[20] Oishi T. Significant relationship between the backward scattering coefficient of sea water and the scatterance at 120. Appl Opt 1990;29(31):4658–65.
[21] Boss E, Pegau WS. Relationship of light scattering at an angle in the backward direction to the backscattering coefficient. Appl Opt 2001;40:5503–7.
[22] Zhang X, Boss E, Gray DJ. Significance of scattering by oceanic particles at angles around 120 degree. Opt Express 2014;22(25):31329–36.
[23] Zhang X, Fournier GR, Gray DJ. Interpretation of scattering by oceanic particles around 120 degrees and its implication in ocean color studies. Opt Express 2017;25(4):A191–9.
[24] Bidigare RR, Morrow JH, Kiefer DA. Derivative analysis of spectral absorption by photosynthetic pigments in the western Sargasso Sea. J Mar Res 1989;47:323–41.
[25] Gordon HR, Morel AY. Remote assessment of ocean color for interpretation of satellite visible imagery: a review. Springer Science & Business Media; 1983.
[26] Loisel H, Morel A. Light scattering and chlorophyll concentration in case 1 waters:a reexamination. Limnol Oceanogr 1998;43:847–58.
[27] Behrenfeld MJ, Boss E, Siegel DA, Shea DM. Carbon-based ocean productivity and phytoplankton physiology from space. Glob Biogeochem Cycles 2005;19.
[28] Morel A, Bricaud A. Inherent optical properties of algal cells including picoplankton: theoretical and experimental results. Can Bull Fish Aquat Sci 1986;214:521–59.
[29] Morel A, Ahn YH. Optical efficiency factors of free-living marine bacteria: Influence of bacterioplankton upon the optical properties and particulate organic carbon in oceanic waters. J Mar Res 1990;48(1):145–75.
[30] Morel A, Ahn YH. Optics of heterotrophic nanoflagellates and ciliates: a tentative assessment of their scattering role in oceanic waters compared to those of bacterial and algal cells. J Mar Res 1991;49(1):177–202.
[31] Ahn Y-H, Bricaud A, Morel A. Light backscattering efficiency and related properties of some phytoplankters. Deep Sea Res Part A. Oceanogr Res Pap 1992;39:1835–55.
[32] Stramski D, Mobley CD. Effects of microbial particles on oceanic optics: a database of single-particle optical properties. Limnol Oceanogr 1997;42(3):538–49.
[33] Stramski D, Bricaud A, Morel A. Modeling the inherent optical properties of the ocean based on the detailed composition of the planktonic community. Appl Opt 2001;40:2929–45.
[34] Kitchen JC, Zaneveld JRV. A three-layered sphere model of the optical properties of phytoplankton. Limnol Oceanogr 1992;37(8):1680–90.
[35] Zaneveld JRV, Kitchen JC. The variation in the inherent optical properties of phytoplankton near an absorption peak as determined by various models of cell structure. J Geophys Res Oceans 1995;100(C7):13309–20.
[36] Stramski D, Piskozub J. Estimation of scattering error in spectrophotometric measurements of light absorption by aquatic particles from three-dimensional radiative transfer simulations. Appl Opt 2003;42:3634–46.
[37] Quirantes A, Bernard S. Light scattering by marine algae: two-layer spherical and nonspherical models. J Quant Spectrosc Radiat Transf 2004;89(1):311–21.
[38] Vaillancourt RD, Brown CW, Guillard RR, Balch WM. Light backscattering properties of marine phytoplankton: relationships to cell size, chemical composition and taxonomy. J Plankton Res 2004;26(2):191–212.
[39] Clavano WR, Boss E, Karp-Boss L. Inherent optical properties of non-spherical marine-like particles - from theory to observations. Oceanogrand Mar Biol Ann Rev 2007;45:1–38.
[40] Stramski D, Boss E, Bogucki D, Voss KJ. The role of seawater constituents in light backscattering in the ocean. Prog Oceanogr 2004;61(1):27–56.
[41] Whitmire AL, Pegau WS, Karp-Boss L, Boss E, Cowles TJ. Spectral backscattering properties of marine phytoplankton cultures. Opt Express 2010;18:15073–93.
[42] Stramski D, Kiefer DA. Light scattering by microorganisms in the open ocean. Prog Oceanogr 1991;28(4):343–83.
[43] Bohren CF, Singham SB. Backscattering by nonspherical particles: a review of methods and suggested new approaches. J Geophys Res Atmos 1991;96(D3):5269–77.
[44] Bricaud A, Zaneveld JRV, Kitchen JC. 1992, December. Backscattering efficiency of coccolithophorids: use of a three-layered sphere model. In: Proceedings of the International Society for Optics and Photonics San Diego, (27–33).
[45] Bernard S, Probyn TA, Quirantes A. Simulating the optical properties of phytoplankton cells using a two-layered spherical geometry. Biogeosci Discuss 2009;6(1).
[46] Dall'Olmo G, Westberry TK, Behrenfeld MJ, Boss E, Slade WH. Significant contribution of large particles to optical backscattering in the open ocean. Biogeosciences 2009;6(6):947–67.
[47] Martinez-Vicente V, Tilstone GH, Sathyendranath S, Miller PI, Groom SB. Contributions of phytoplankton and bacteria to the optical backscattering coefficient over the Mid-Atlantic Ridge. Mar Ecol Prog Ser 2012;445:37–51.
[48] Huot Y, Morel A, Twardowski MS, Stramski D, Reynolds RA. Particle optical backscattering along a chlorophyll gradient in the upper layer of the eastern South Pacific Ocean. Biogeosci Discuss 2007;4(6):4571–604.
[49] Hillebrand H, Dürselen CD, Kirschtel D, Pollingher U, Zohary T. Biovolume calculation for pelagic and benthic microalgae. J Phycol 1999;35(2):403–24.
[50] Sun J, Liu D. Geometric models for calculating cell biovolume and surface area for phytoplankton. J Plankton Res 2003;25(11):1331–46.
[51] Waterman PC. Symmetry, unitarity, and geometry in electromagnetic scattering. Phys Rev D 1971;3(4):825.
[52] Mishchenko MI. Calculation of the amplitude matrix for a nonspherical particle in a fixed orientation. Appl Opt 2000;39(6):1026–31.
[53] Zhai PW, Hu Y, Trepte CR, Winker DM, Josset DB, Lucker PL, Kattawar GW. Inherent optical properties of the coccolithophore: Emiliania huxleyi. Opt Express 2013;21(15):17625–38.
[54] Gordon HR, Du T. Light scattering by nonspherical particles: application to coccoliths detached from Emiliania huxleyi. Limnol Oceanogr 2001;46(6):1438–54.
[55] Gordon HR. Backscattering of light from disklike particles: is fine-scale structure or gross morphology more important? Appl Opt 2006;45(27):7166–73.
[56] Bi L, Yang P. Impact of calcification state on the inherent optical properties of Emiliania huxleyi coccoliths and coccolithophores. J Quant Spectrosc Radiat Transf 2015;155:10–21.
[57] Dauchet J, Blanco S, Cornet JF, Fournier R. Calculation of the radiative properties of photosynthetic microorganisms. J Quant Spectrosc Radiat Transf 2015;161:60–84.
[58] Bi L, Yang P, Kattawar GW, Kahn R. Modeling optical properties of mineral aerosol particles by using nonsymmetric hexahedra. Appl Opt 2010;49(3):334–42.
[59] Sun B, Yang P, Kattawar GW, Zhang X. Physical-geometric optics method for large size faceted particles. Opt Express 2017;25(20):24044–60.
[60] Xu G, Sun B, Brooks SD, Yang P, Kattawar GW, Zhang X. Modeling the inherent optical properties of aquatic particles using an irregular hexahedral ensemble. J Quant Spectrosc Radiat Transf 2017;191:30–9.
[61] Zhang X, Huot Y, Gray DJ, Weidemann A, Rhea WJ. Biogeochemical origins of particles obtained from the inversion of the volume scattering function and spectral absorption in coastal waters. Biogeosciences 2013;10(9):6029.
[62] Zhang X, Gray DJ. Backscattering by very small particles in coastal waters. J Geophys Res Oceans 2015;120(10):6914–26.
[63] Xu YL, Gustafson BÅ. A generalized multiparticle Mie-solution: further experimental verification. J Quant Spectrosc Radiat Transf 2001;70(4):395–419.
[64] Quirantes A, Bernard S. Light-scattering methods for modeling algal particles as a collection of coated and/or nonspherical scatterers. J Quant Spectrosc Radiat Transf 2006;100(1):315–24.
[65] Meyer RA. Light scattering from biological cells: dependence of backscatter radiation on membrane thickness and refractive index. Appl Opt 1979;18(5):585–8.
[66] Quinby-Hunt MS, Hunt AJ, Lofftus K, Shapiro D. Polarized-light scattering studies of marine Chlorella. Limnol Oceanogr 1989;34(8):1587–600.
[67] Moutier W, Duforêt-Gaurier L, Thyssen M, Loisel H, Mériaux X, Courcot L, Dessailly D, Alvain S. Scattering of individual particles from cytometry: tests on phytoplankton cultures. Opt Express 2016;24(21):24188–212.
[68] Matthews MW, Bernard S. Characterizing the absorption properties for remote sensing of three small optically-diverse South African reservoirs. Remote Sens 2013;5(9):4370–404.
[69] Meyer RA, Brunsting ALBERT. Light scattering from nucleated biological cells. Biophys J 1975;15(3):191–203.
[70] Bricaud A, Morel A. Light attenuation and scattering by phytoplanktonic cells: a theoretical modeling. Appl Opt 1986;25(4):571–80.
[71] Bricaud A, Bédhomme AL, Morel A. Optical properties of diverse phytoplanktonic species: experimental results and theoretical interpretation. J Plankton Res 1988;10(5):851–73.
[72] Aas E. Refractive index of phytoplankton derived from its metabolite composition. J Plankton Res 1996;18(12):2223–49.
[73] Stramski D, Morel A. Optical properties of photosynthetic picoplankton in different physiological states as affected by growth irradiance. Deep Sea Res Part A. Oceanogr Res Pap 1990;37(2):245–66.
[74] Stramski D, Reynolds RA. Diel variations in the optical properties of a marine diatom. Limnol Oceanogr 1993;38(7):1347–64.
[75] Stramski D, Shalapyonok A, Reynolds RA. Optical characterization of the oceanic unicellular cyanobacterium Synechococcus grown under a day-night cycle in natural irradiance. J Geophys Res Oceans 1995;100(C7):13295–307.
[76] Hodgson RT, Newkirk DD. Pyridine immersion: a technique for measuring the refractive index of marine particles. In: Proceedings of the ocean optics; 1975. p. 19–20. August.
[77] Hulst vande. Light scattering by small particles, 470. New York: Wiley; 1957.
[78] Stramski D, Morel A, Bricaud A. Modeling the light attenuation and scattering by spherical phytoplanktonic cells: a retrieval of the bulk refractive index. Appl Opt 1988;27(19):3954–6.
[79] Campbell JW. The lognormal distribution as a model for bio-optical variability in the sea. J Geophys Res Oceans 1995;100(C7):13237–54.
[80] Zhang X, Gray DJ, Huot Y, You Y, Bi L. Comparison of optically derived particle size distributions: scattering over the full angular range versus diffraction at near forward angles. Appl Opt 2012;51(21):5085–99.

[81] Bader H. The hyperbolic distribution of particle sizes. J Geophys Res 1970;75(15):2822–30.
[82] Brown OB, Gordon HR. Size–refractive index distribution of clear coastal water particulates from light scattering. Appl Opt 1974;13(12):2874–81.
[83] Kitchen JC, Zaneveld JRV. On the noncorrelation of the vertical structure of light scattering and chlorophyll α in case I waters. J Geophys Res Oceans 1990;95(C11):20237–46.
[84] Claustre H, Bricaud A, Babin M, Bruyant F, Guillou L, Le Gall F, Marie D, Partensky F. Diel variations in Prochlorococcus optical properties. Limnol Oceanogr 2002;47(6):1637–47.
[85] Ohi N, Ishiwata Y, Taguchi S. Diel patterns in light absorption and absorption efficiency factors of isochrysis galbana (prymnesiophyceae) 1. J Phycol 2002;38(4):730–7.
[86] Poulin C, Antoine D, Huot Y. Diurnal variations of the optical properties of phytoplankton in a laboratory experiment and their implication for using inherent optical properties to measure biomass. Opt Express 2018;26(2):711–29.
[87] Welschmeyer NA. Fluorometric analysis of chlorophyll a in the presence of chlorophyll *b* and pheopigments. Limnol Oceanogr 1994;39(8):1985–92.
[88] MacIntyre HL, Cullen JJ. Using cultures to investigate the physiological ecology of microalgae. Algal Cultur Tech 2005:287–326.
[89] Zhang X, Hu L, He MX. Scattering by pure seawater: effect of salinity. Opt Express 2009;17(7):5698–710.
[90] Sullivan JM, Twardowski MS, Ronald J, Zaneveld V, Moore CC. Measuring optical backscattering in water. Light Scatter Rev 2013;7:189–224.
[91] Hildebrand M, York E, Kelz JI, Davis AK, Frigeri LG, Allison DP, Doktycz MJ. Nanoscale control of silica morphology and three-dimensional structure during diatom cell wall formation. J Mater Res 2006;21(10):2689–98.
[92] Godoi RHM, Aerts K, Harlay J, Kaegi R, Ro CU, Chou L, Van Grieken R. Organic surface coating on Coccolithophores-Emiliania huxleyi: Its determination and implication in the marine carbon cycle. Microchem J 2009;91(2):266–71.
[93] Zhang X. 2009, ZhangMie [Matlab function] Accessed January 2017.
[94] Bi L, Yang P, Kattawar GW, Kahn R. Modeling optical properties of mineral aerosol particles by using nonsymmetric hexahedra. Appl Opt 2010;49(3):334–42.
[95] Jonasz M. Nonsphericity of suspended marine particles and its influence on light scattering. Limnol Oceanogr 1987;32(5):1059–65.
[96] Witkowski K, Woliński L, Turzyński Z, Gedziorowska D, Zielifiski A. The investigation of kinetic growth of Chlorella vulgaris cells by the method of integral and dynamic light scattering. Limnol Oceanogr 1993;38(7):1365–72.
[97] Witkowski K, Król T, Zieliriński A, Kuteń E. A light-scattering matrix for unicellular marine phytoplankton. Limnol Oceanogr 1998;43(5):859–69.
[98] Janssen M, Bathke L, Marquardt J, Krumbein WE, Rhiel E. Changes in the photosynthetic apparatus of diatoms in response to low and high light intensities. Int Microbiol 2001;4(1):27–33.
[99] Volten H, De Haan JF, Hovenier JW, Schreurs R, Vassen W, Dekker AG, Hoogenboom HJ, Charlton F, Wouts R. Laboratory measurements of angular distributions of light scattered by phytoplankton and silt. Limnol Oceanogr 1998;43(6):1180–97.
[100] Voss KJ, Balch WM, Kilpatrick KA. Scattering and attenuation properties of Emiliania huxleyi cells and their detached coccoliths. Limnol Oceanogr 1998;43(5):870–6.
[101] Moutier W, Duforêt-Gaurier L, Thyssen M, Loisel H, Mériaux X, Courcot L, Dessailly D, Rêve AH, Grégori G, Alvain S, Barani A. Evolution of the scattering properties of phytoplankton cells from flow cytometry measurements. PloS One 2017;12(7):e0181180.
[102] Ackleson SG, Cullen JJ, Brown J, Lesser M. Irradiance-induced variability in light scatter from marine phytoplankton in culture. J Plankton Res 1993;15(7):737–59.
[103] Svensen Ø, Frette Ø, Erga SR. Scattering properties of microalgae: the effect of cell size and cell wall. Appl Opt 2007;46(23):5762–9.
[104] Fernández E, Marañón E, Balch WM. Intracellular carbon partitioning in the coccolithophorid Emiliania huxleyi. J Mar Syst 1996;9(1–2):57–66.
[105] Ackleson SG, Spinrad RW, Yentsch CM, Brown J, Korjeff-Bellows W. Phytoplankton optical properties: flow cytometric examinations of dilution-induced effects. Appl Opt 1988;27(7):1262–9.
[106] Green RE, Sosik HM, Olson RJ. Contributions of phytoplankton and other particles to inherent optical properties in New England continental shelf waters. Limnol Oceanogr 2003;48(6):2377–91.
[107] Duforêt-Gaurier L, Moutier W, Guiselin N, Thyssen M, Dubelaar G, Mériaux X, Courcot L, Dessailly D, Loisel H. Determination of backscattering cross section of individual particles from cytometric measurements: a new methodology. Opt Express 2015;23(24):31510–33.
[108] Agagliate J, Röttgers R, Twardowski MS, McKee D. Evaluation of a flow cytometry method to determine size and real refractive index distributions in natural marine particle populations. Appl Opt 2018;57(7):1705–16.